



Function and firing of the *Streptomyces coelicolor* contractile injection system requires the membrane protein CisA

Reviewed Preprint

v1 • January 6, 2025

Not revised

Bastien Casu, Joseph W Sallmen, Peter E Haas, Govind Chandra, Pavel Afanasyev, Jingwei Xu, Susan Schlimpert , Martin Pilhofer 

Department of Biology, Institute of Molecular Biology & Biophysics, Eidgenössische Technische Hochschule Zürich, Zürich, Switzerland • John Innes Center, Department of Molecular Microbiology, Norwich Research Park, Norwich, United Kingdom

 https://en.wikipedia.org/wiki/Open_access

 Copyright information

eLife Assessment

This **valuable** study provides insights into the structure and function of bacterial contractile injection systems that are present in the cytoplasm of many *Streptomyces* strains. A **convincing** high-resolution model of the structure of extended forms of the cytoplasmic contractile injection system assembly from *Streptomyces coelicolor* is presented, with some investigation of the membrane protein CisA in attachment of the extended assembly to the inner face of the cytoplasmic membrane and the firing of the system. The work expands the current understanding of these diverse bacterial nanomachines.

<https://doi.org/10.7554/eLife.104064.1.sa4>

Abstract

Bacterial contractile injection systems (CIS) are phage tail-like macromolecular complexes that mediate cell-cell interactions by injecting effector proteins into target cells. CIS from *Streptomyces coelicolor* (CIS^{Sc}) are localized in the cytoplasm. Under stress, they induce cell death and impact the bacteria's life cycle. It remains unknown whether CIS^{Sc} require accessory proteins to directly interact with the cytoplasmic membrane and function.

Here, we characterize the putative membrane adaptor CisA, a conserved factor in *CIS* gene clusters across *Streptomyces* species. We show by cryo-electron tomography imaging and *in vivo* assays that CIS^{Sc} contraction and function depend on CisA. Using single-particle cryo-electron microscopy, we provide an atomic model of the extended CIS^{Sc} apparatus; however, CisA is not part of the complex. Instead, our findings show that CisA is a membrane protein with a cytoplasmic N-terminus predicted to interact with CIS^{Sc} components, thereby providing a possible mechanism for mediating CIS^{Sc} recruitment to the membrane and subsequent firing.

Our work shows that CIS function in multicellular bacteria is distinct from Type 6 Secretion Systems and extracellular CIS, and possibly evolved due to the role CIS^{Sc} play in regulated cell death.

Introduction

Bacteria employ different types of contractile injection systems (CIS) to mediate cell-cell interactions or to mediate cell death (1). CIS are evolutionarily and structurally related to contractile tails of bacteriophages and are comprised of core modules including a baseplate, a contractile sheath, and an inner tube (2,3). CIS firing is triggered by a conformational change within the baseplate (4,5) and results in the contraction of the sheath, which in turn propels the inner tube along with the spike tip. Tube expulsion facilitates the release of associated effector proteins into target cells or the extracellular space (6,7).

Bioinformatic analyses have shown that CISs are conserved across diverse microbial phyla, including Gram-negative and Gram-positive bacteria, as well as archaea (8,9). Based on their distinct modes of action, CIS can be categorized into two main groups: intracellular type VI secretion systems (T6SS) and extracellular CIS (eCIS). T6SS are abundant among Gram-negative bacteria and in some archaea, and they are anchored to the cytoplasmic membrane during assembly and firing (10–12). A crucial component of the T6SS is the baseplate, which acts as a nucleus for T6SS assembly and mediates the binding of the T6SS particles to the cytoplasmic membrane until contraction. Upon contraction, the spike and inner tube are propelled out of the cell into an adjacent cell or the medium. eCIS, on the other hand, are assembled as free-floating particles in the cytoplasm and are subsequently released into the extracellular space upon lysis of the producer cell (13–16). Following the release, eCIS attach to the surface of target cells via their tail fibers, followed by contraction and puncturing of the target cell envelope.

Besides T6SS and eCIS, there is accumulating evidence of additional CIS assemblies with distinct modes of action in bacteria. For example, in multicellular cyanobacteria, CIS are anchored to the intracellular thylakoid membrane stacks via an extension of the baseplate components and have been proposed to function in cell lysis and the formation of “ghost cells” in response to stress conditions (17). Furthermore, several recent studies reported the production of free-floating cytoplasmic CIS particles in the multicellular Gram-positive *Streptomyces* bacteria, which have been shown to modulate cellular development through presumably slightly different mechanisms (18–22).

Streptomyces are best known for producing a plethora of medically and industrially important secondary metabolites, including molecules with antimicrobial, antifungal, anticancer or immunosuppressive properties. The production of these molecules is tightly coordinated with the *Streptomyces* developmental life cycle that encompasses two filamentous cell types: vegetative hyphae that grow by tip extension and branching to scavenge for nutrients, and reproductive (aerial) hyphae that eventually differentiate into chains of spores, which can then be dispersed to restart the life cycle (23,24). Using *Streptomyces coelicolor* as a model organism, we and others previously demonstrated that *S. coelicolor* CIS (CIS^{Sc}) mediate a form of regulated cell death, which influences the onset of sporulation and secondary metabolite production in response to exogenous stress and unknown cellular signals (Figure 1a) (18,19).

It remains unclear whether CIS^{Sc} contraction occurs while the CIS^{Sc} particles are free-floating in the cytoplasm or whether this depends on an interaction with the membrane. Moreover, CIS encoded in *Streptomyces* genomes lack clear homologs for tail fiber components or a T6SS trans-envelope complex, raising the question of how CIS^{Sc} particles could potentially interact with the cytoplasmic membrane. We and others recently noted an uncharacterized protein (18,19),

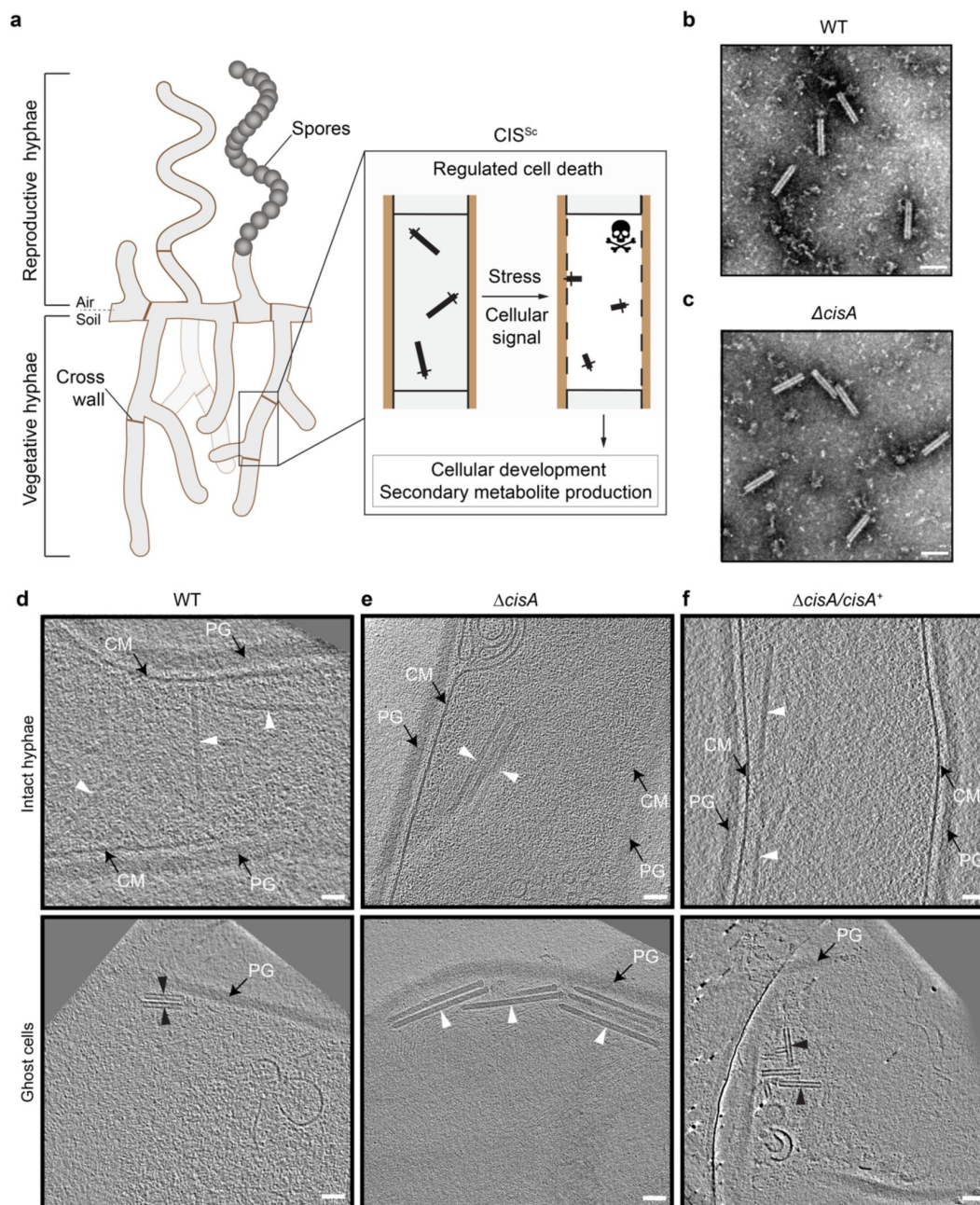


Figure 1

Contraction of CIS^{Sc} *in situ* is dependent on Cisa.

a. Schematic of the mode of action of CIS^{Sc} in *Streptomyces coelicolor* (18,19). CIS^{Sc} are assembled as free-floating particles in the cytoplasm of vegetative hyphae. In response to cellular stress and/or an unknown cellular signal, CIS^{Sc} particles contract, which results in regulated cell death (mediated by released effectors) and impacts cellular development.

b/c. Negative-stain electron micrographs of purified CIS^{Sc} particles from *S. coelicolor* wildtype (WT) (b) and the $\Delta cisa$ mutant (c), show that all CIS^{Sc} particles are contracted upon purification. These experiments were performed three independent times. Bars, 100 nm.

d-f. Shown are representative images of cryo-electron tomogram slices (thickness 11 nm) of vegetative hyphae (top: intact cells; bottom: ghost cells) of *S. coelicolor* WT (d), $\Delta cisa$ mutant (e), and the complemented $\Delta cisa/cisa^+$ mutant (f). CIS^{Sc} particles remain almost exclusively in an extended state (white arrowheads) in the $\Delta cisa$ mutant, whereas in ghost cells derived from the WT and the complemented mutant, CIS^{Sc} particles (black arrowheads) are mostly contracted. See also **Supplementary Fig. 1**. PG, peptidoglycan; CM, cytoplasmic membrane; Bars, 50 nm.

SCO4242, which is conserved in the majority of *Streptomyces* species and other Actinomycete species that carry a type IId eCIS locus (8,9) (Supplementary Fig. 1 and Supplementary Data 1 and 2). Interestingly, SCO4242 is encoded just downstream of the baseplate components in the CIS^{Sc} gene cluster, a location that usually encodes tail fibers from conventional eCIS (13,16,25). We will, therefore, refer to the gene product of SCO4242 as CisA for “CIS^{Sc}-associated protein A.” Here, we set out to assess the importance of CisA for CIS^{Sc} function and its possible role as a membrane anchor.

Results

CisA is required for CIS^{Sc} contraction *in situ*

To explore the role of CisA (SCO4242) in CIS^{Sc} contraction and function, we first generated an *S. coelicolor* Δ *cisA* null mutant. Negative stain electron microscopy (EM) imaging of CIS^{Sc} particles that were purified from Δ *cisA* mutant cells showed assemblies in the contracted conformation, similar to the CIS particles purified from the wild type (WT) (Fig. 1b/c). We then imaged vegetative hyphae of the WT, the Δ *cisA* mutant and the complemented mutant (Δ *cisA/cisA*⁺) by cryo-electron tomography (cryoET) (270 tomograms in total, n=3 experiments). The observed CIS^{Sc} particles in intact hyphae of these three imaged strains did not reveal discernable differences, indicating that CisA is not required for CIS^{Sc} assembly. We previously showed that CIS^{Sc} contraction is linked to cell death in *S. coelicolor* wildtype hyphae and we observed a clear shift in the number of extended to fully contracted CIS^{Sc} particles in damaged and dead hyphae (ghost cells) (18). Interestingly, and in contrast to the WT and complemented *cisA* mutant strain (Fig. 1d and f), *cisA*-deficient hyphae only contained CIS^{Sc} particles in the extended conformation irrespective of the cellular integrity of the hyphae (Fig. 1e, Supplementary Fig. 2a-d). While hyphal cell death can be induced by a range of different external or internal factors, our results suggest that CisA is required for the contraction of CIS^{Sc} *in situ*.

CryoEM structure of the extended CIS^{Sc} assembly

Contractile injection systems are generally classified into intracellular type VI secretions systems (T6SS) and the superfamily of extracellular CIS (eCIS), which is subdivided into six families with distinct genetic compositions (8). Many *Streptomyces* genomes contain a class IId eCIS locus, a subtype that is structurally less well understood compared to other eCIS subtypes, which includes ‘antifeeding prophages’ (AFPs) from *Serratia*, ‘metamorphosis-associated contractile structures’ (MACs) from *Pseudoalteromonas luteoviolacea*, AlgoCIS from *A. machipongonensis* or ‘*Photorhabdus* virulence cassettes’ (PVCs) from *P. asymbiotica* (1).

The CIS^{Sc} gene cluster consists of 19 predicted open reading frames (accessions SCO4242-4260) (Fig. 2a), including genes with sequence similarities to potential CIS structural components (*cis1-cis16*), as well as additional genes with unknown functions (including *cisA*) (18,19). To determine whether CisA is an integral component of CIS^{Sc}, we set out to elucidate the high-resolution structure of purified CIS^{Sc} particles from a non-contractile CIS^{Sc} mutant (18). The purified assemblies were subjected to single particle cryo-electron microscopy (cryoEM) for structure determination (Supplementary Fig. 3), yielding the first high-resolution model of the CIS^{Sc} in its extended conformation, which also presents the first example of a CIS IId subtype (8).

Our model shows that extended CIS^{Sc} particles share the conserved eCIS architecture, including three modules: cap, sheath-tube and baseplate (Fig. 2b). We processed the dataset using an established workflow that was previously employed to produce the atomic model for other CIS

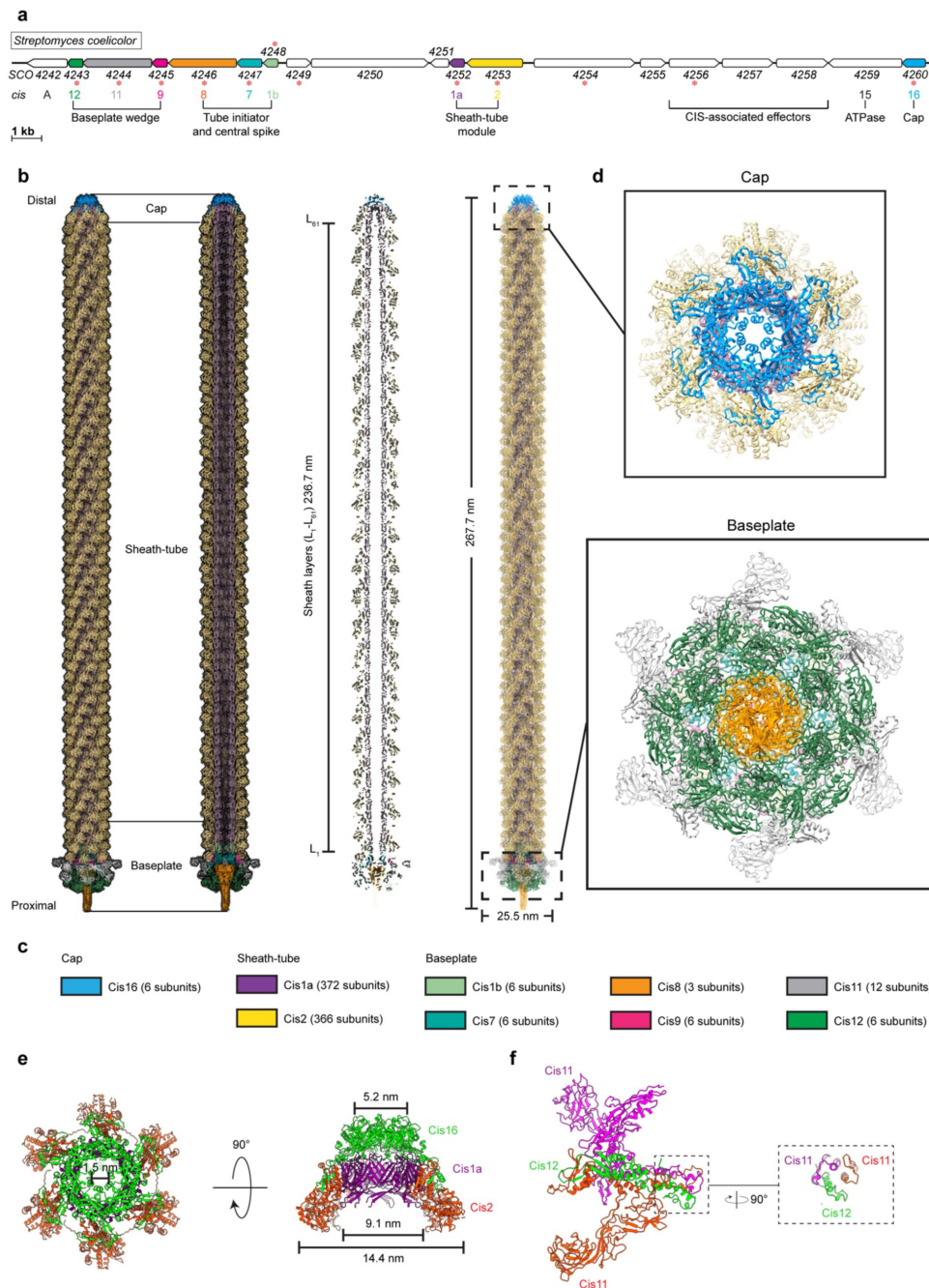


Figure 2

CryoEM structure of the extended CIS^{Sc} assembly reveals its composition.

a. Schematic illustrating the CIS^{Sc} gene cluster (adapted from (18)). Asterisks indicate gene products that were detected by mass spectrometry analyzing crude preparations of CIS^{Sc} particles (red). See also Supplementary Table 1.

b/c. Single-particle cryoEM structure of an extended CIS^{Sc} particle obtained from purified particles from a non-contractile CIS^{Sc} mutant. Shown is the composite atomic model in surface (left) and ribbon (right) rendering (b). Subunits are color-coded according to (a) and their copy numbers in the assembly are indicated in (c).

d. Perpendicular views of the ribbon representation of the CIS^{Sc} model of the cap and baseplate modules.

e. Top view (left) and side view (right) of ribbon diagrams showing the cap module of CIS^{Sc}, revealing that the cap is composed of a Cis16 hexamer.

f. Ribbon diagrams showing a single baseplate wedge subunit, which is composed of two copies of Cis11 and one copy of Cis12.

(**Supplementary Fig. 3**) (13,17). The resulting maps of the baseplate and the cap reached resolutions of 3.5 and 3.4 Å, respectively. The quality of the final maps from the two modules enabled *de novo* structural modelling (**Supplementary Fig. 4**, Supplementary Table 1).

The final model of CIS^{Sc} comprised 783 polypeptide chains that assemble into a bullet-shaped particle measuring 268 nm in length (**Fig. 2b/c**). All analyzed particles were identical in length, consistent with our *in situ* data of extended CIS^{Sc} particles in vegetative hyphae of WT *S. coelicolor* (**Fig. 1d-f**). The length of eCIS particles is often controlled by tape measure proteins (26), we note, however, that the corresponding gene is absent from the CIS^{Sc} gene cluster. The distal end of the CIS^{Sc} is capped by a tail terminator complex (**Fig. 2c/e**). This cap comprises one protein, Cis16, forming a C6-symmetrical complex that terminates the inner tube and sheath, respectively. This minimal architecture resembles the cap complexes of PVC or Pyocin R2 CISs, but it is different from the more complex AlgoCIS from *A. machipongonensis* and AFP from *S. entomophila* (**Supplementary Fig. 5**) (13,16,25,27). The structures of the CIS^{Sc} sheath-tube module have been discussed previously (18). Here we found that the module consists of 61 sheath layers (Cis2-L₁-L₆₁) and 60 tube layers (Cis1-L₁-L₆₀) (**Fig. 2b/d**).

The baseplate module comprises a heteromeric assembly of the proteins Cis1b/7/8/9/11/12 (**Fig. 2b/c**). The symmetry transition from the inner tube (Cis1a, C6) to the VgrG-like spike (Cis8, C3) is adapted by two layers of the tube initiators Cis1b and Cis7. The first layer of the sheath (Cis2) is bound to the conserved gp25-like protein Cis9, which connects to the baseplate ‘wedges’ composed of Cis11 and Cis12 (**Fig. 2b/c**). Importantly, the CIS^{Sc} ‘wedges’ consist of two copies of Cis11 and one copy of Cis12 (**Fig. 2f**), resembling the baseplate of Pyocin R2 (27). This is in contrast to other previously reported eCIS, whose baseplate wedge comprises only one Cis11/12 component (AlgoCIS, AFP, PVC) and a Cis11 extension forming a cage around the spike (AlgoCIS) (**Supplementary Fig. 6**) (13,16,25).

Out of the 19 predicted open reading frames in the CIS^{Sc} gene cluster (**Fig. 2a**), nine encoded proteins were present in the final reconstruction, all with atomic models built (**Fig. 2b/c**). However, we did not detect a density for CisA in our model, suggesting that CisA is not part of purified CIS^{Sc} particles but may interact via a different mechanism. This is also in agreement with mass spectrometry results that indicate the absence of CisA peptides from purified CIS^{Sc} particles (**Fig. 2a**) (18). We speculate that the purification protocol used to isolate CIS^{Sc} particles for single-particle analysis may not preserve a CIS^{Sc}-CisA interaction, or the interaction is too transient and only occurs under certain growth conditions. To better understand how CisA may mediate CIS^{Sc} function, we set out to further characterize CisA *in vivo*.

CisA is a bitopic protein

Previous bioinformatic analyses (18,19) and AlphaFold2 (28) modeling of CisA suggest that CisA consists of a largely unstructured N-terminal region, a transmembrane segment, and a conserved immunoglobulin-like (IgG) domain at the C-terminus (**Fig. 3a**). To characterize the intracellular localization of CisA, we first generated a strain in which *cisA* was fused to the N-terminus of *mCherry* and expressed *in trans* from a constitutive promoter in the *S. coelicolor* Δ *cisA* mutant. Using fluorescence light microscopy, we consistently observed a CisA-mCherry fluorescence signal along the hyphal periphery, indicative of a membrane-associated protein (**Fig. 3b**). In contrast, no fluorescence was observed in WT hyphae carrying an empty plasmid (**Fig. 3c**). Next, we tested if CisA is indeed localized to the membrane *in vivo* by performing cellular fractionation experiments. We separated soluble proteins from membrane proteins using whole cell lysates from the *S. coelicolor* WT or the Δ *cisA* mutant that was complemented with a *cisA*-3xFLAG fusion expressed *in trans* from a constitutive promoter. Our analysis confirmed that CisA-3xFLAG co-sedimented with the cell membranes, while the cytoplasmic transcription factor WhiA could only be detected in the soluble protein fraction (**Fig. 3d**).

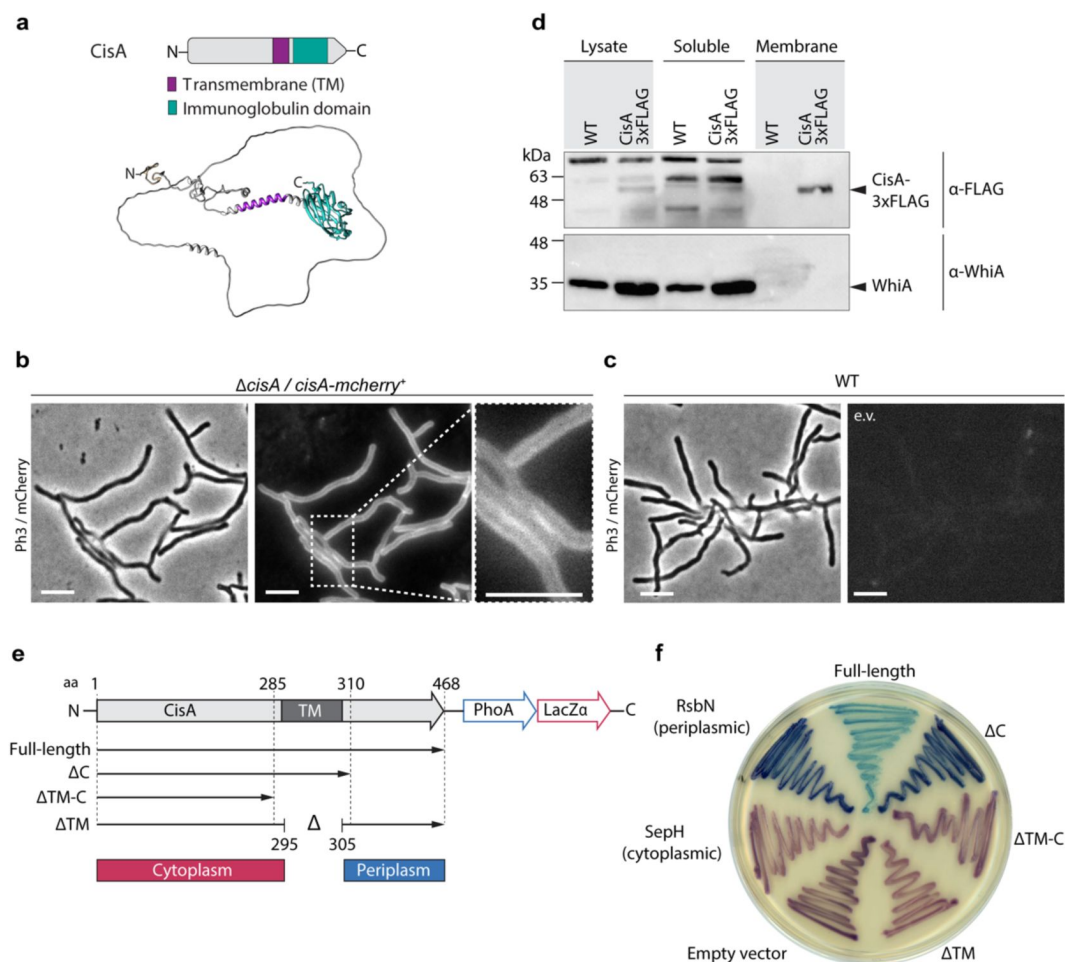


Figure 3

CisA is a single-pass membrane protein.

a. Schematic and AlphaFold2 model of CisA. CisA is predicted to contain a largely unstructured N-terminal domain (grey), a transmembrane domain (TM, purple) and a C-terminal immunoglobulin-like domain (green).

b/c. Representative micrographs (left panels: phase contrast, Ph3; right panel: mCherry) of strains of *S. coelicolor* vegetative hyphae either constitutively expressing CisA-mCherry ($\Delta cisA/cisA\text{-mCherry}$) *in trans* (b) or WT cells carrying an empty vector (e.v.) to control for background fluorescence (c). Box shows a magnified region of hyphae with CisA-mCherry accumulation in the cellular periphery. Bars, 5 μm .

d. Western blot of the cellular fractionation of samples from the *S. coelicolor* WT or the $\Delta cisA$ mutant constitutively expressing a CisA-3xFLAG fusion *in trans*. Lysate and soluble and membrane fractions were probed for the presence of CisA-3xFLAG with an α -FLAG antibody (top). Fractionation efficiency was assessed using an α -WhiA antibody to detect the soluble transcription factor WhiA (bottom). CisA-3xFLAG was detected in the lysate and the membrane fraction. The experiment was performed in biological duplicates and shown is a representative image.

e/f. Experimental determination of the CisA membrane topology using the dual *phoA-lacZa* reporter in *E. coli*. The schematic diagram (e) depicts the four CisA constructs used in the assay and indicates the relevant amino acid (aa) deleted in the three CisA mutant derivatives. The analysis of colony coloration (f); pink coloration for cytosolic proteins and blue coloration for periplasmic proteins, indicates that the CisA N-terminus is localized in the cytoplasm and the CisA C-terminus localized to the periplasm and this topology is dependent on the transmembrane domain (TM). *E. coli* strains carrying an empty reporter plasmid or reporter plasmids with the *Streptomyces* genes for SepH (cytoplasmic) and RsbN (periplasmic) were used as controls. Note that expression of full-length CisA in *E. coli* is toxic, leading to reduced growth and lighter blue coloration.

Next, we investigated the topology of CisA in the membrane using a dual *phoA-lacZ* reporter system in *E. coli*. The reporter activity can be directly visualized on indicator plates based on the complementary activities of the cytoplasmic reporter β -galactosidase LacZ (magenta coloration) and the periplasmic reporter alkaline phosphatase PhoA (blue coloration) (29). We engineered *E. coli* strains that expressed a C-terminal fusion of CisA variants to the PhoA-LacZ reporter, including full-length CisA and CisA variants that carried either a deletion in the predicted transmembrane domain and/or the putative periplasmic domain (Fig. 3e). In addition, we included three controls, including 1) cells carrying the empty reporter plasmid, resulting only in cytoplasmic β -galactosidase activity, 2) cells expressing a PhoA/LacZ fusion to the *Streptomyces* cytoplasmic cell division protein SepH, and 3) cells expressing a PhoA/LacZ fusion to the periplasmic domain of the *Streptomyces* membrane protein RsbN (30,31). The results of this assay confirmed that CisA is a bitopic protein with an N-terminus (amino acids 1-285) located in the cytoplasm and a C-terminus (amino acids 310-468) present in the periplasm of *E. coli* (Fig. 3f).

Collectively, our results demonstrate that CisA is a membrane protein comprised of a flexible, cytoplasmic N-terminal domain and a C-terminal globular IgG-like domain that is exposed to the outside of the cytoplasmic membrane.

CisA is essential for the cellular function of CIS^{Sc}

We previously established a fluorescence-based assay to demonstrate that the production of functional CIS^{Sc} particles results in a significantly reduced viability of *Streptomyces* hyphae exposed to exogenous stress, including treatment with the membrane-pore forming antibiotic nisin, UV radiation or the protonophore carbonyl cyanide 3-chlorophenylhydrazone (CCCP) (18). This viability assay is based on the measurement of the ratio of two fluorescent markers, namely cytoplasmic sfGFP produced by viable intact hyphae and the membrane dye FM5-95 to detect intact as well as partially lysed hyphae. Using this assay, we tested whether CisA was essential for CIS^{Sc}-mediated cell death. We therefore determined the relative viability of the WT *cisA*, the $\Delta cisA$ and the complemented *cisA* ($\Delta cisA/cisA^+$) strains expressing cytosolic sfGFP. We compared cells exposed to a sublethal concentration of nisin (1 μ g/ml for 90 min) to cells not exposed to antibiotic stress. All three strains were found to express CIS^{Sc} assemblies under these growth conditions (Supplementary Fig. 7).

Without nisin stress, all three strains exhibited a similar sfGFP/FM5-95 ratio, indicating no significant difference in viability (Fig. 4a/c). As previously observed (18), the viability of the WT was dramatically reduced in response to nisin stress. In contrast, the viability of $\Delta cisA$ hyphae was unaffected by nisin stress and comparable to the viability of untreated cells. This phenotype could be completely reversed by complementing the $\Delta cisA$ deletion *in trans* (Fig. 4b/d). Notably, the $\Delta cisA$ strain phenocopies CIS^{Sc} knockout and non-contractile mutants we analyzed previously (18). Thus, we conclude that CisA is required for CIS^{Sc}-mediated cell death upon stress.

To further test the dependence of CIS^{Sc} function on CisA, we conducted additional *in vivo* assays. Previous studies showed that the absence of functional CIS^{Sc} impacted the timely differentiation of *Streptomyces* hyphae into chains of spores, resulting in accelerated cellular development and reduced secondary metabolite production (18,19). Here we repeated these analyses using the WT, the $\Delta cisA$ mutant and the complemented mutant ($\Delta cisA/cisA^+$). All strains consistently completed their life cycle and synthesized spores after 96 h of growth on solid medium (Fig. 4e). Importantly, unlike the WT and the $\Delta cisA/cisA^+$ strain, $\Delta cisA$ mutant colonies sporulated markedly earlier (72 h). These findings were further corroborated by quantifying the number of spores produced by each strain under the same experimental conditions (Fig. 4f). Finally, we also tested the production of the two characteristic pigmented secondary metabolites of *S. coelicolor*, actinorhodin (blue) (32) and undecylprodigiosin (red) (33). Compared to the WT and the $\Delta cisA/cisA^+$ strain, the $\Delta cisA$ mutant showed significantly reduced levels of secondary metabolite

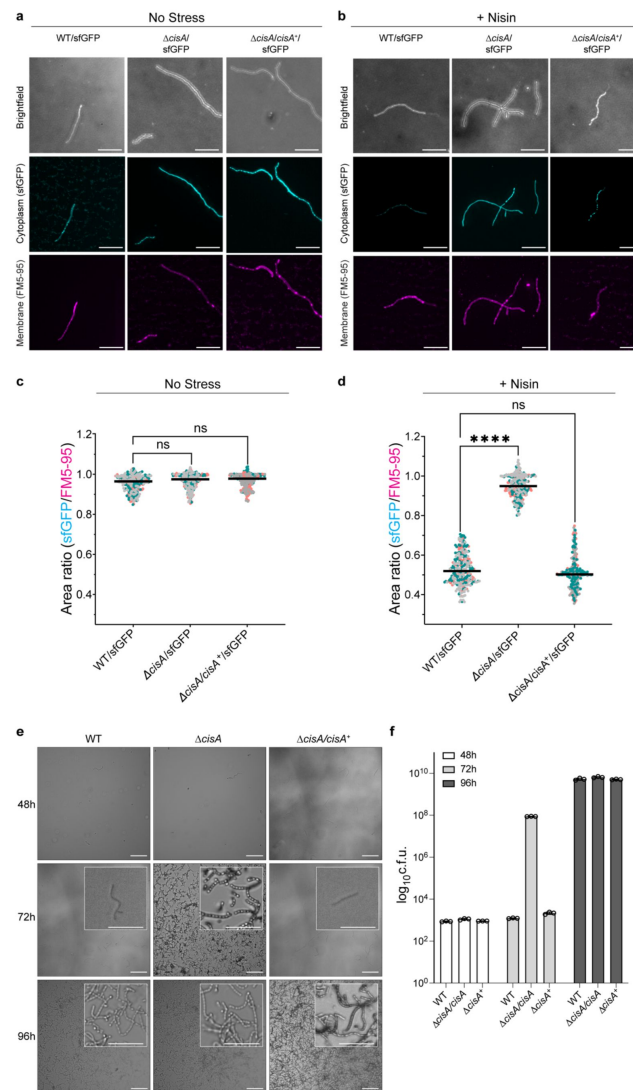


Figure 4

CisA is required for regulated cell death and cellular function of CIS^{Sc}.

a-d. Light microscopy-based viability assay showing that CIS^{Sc} do not mediate cell death in CisA-deficient hyphae in response to exogenous stress. Shown are representative micrographs of the WT/sfGFP, the $\Delta cisA$ /sfGFP and the complemented $\Delta cisA/cisA^+$ /sfGFP mutant expressing cytosolic sfGFP (indicator for live cells). Strains were grown for 48 h and then either incubated without (a) or with (b) the membrane-disrupting antibiotic nisin (1 $\mu\text{g}/\text{ml}$ nisin for 90 min). Samples were subsequently stained with the fluorescent membrane dye FM5-95 to visualize the cytoplasmic membrane. Bars, 10 μm . Z-stacks were taken of the samples and the relative fluorescence ratio from sfGFP to FM5-95 was calculated in c/d. WT and $\Delta cisA/cisA^+$ complemented cells showed a significantly higher rate of cell death in response to nisin treatment than $\Delta cisA$ cells. There is no significant difference in the viability of the tested strains in the absence of nisin. Experiments were performed in three biological replicates (green, grey and pink data points). Black lines indicate the mean ratio derived from biological triplicate experiments ($n=100$ images per replicate). ns (not significant) and **** ($p < 0.0001$) were determined using a one-way ANOVA and Tukey's post-test.

e. Visualization of spore production in WT, $\Delta cisA$ mutant and $\Delta cisA/cisA^+$ mutant reveal accelerated cellular development of the $\Delta cisA$ mutant. Shown are representative brightfield images of surface impressions of plate-grown colonies of each strain taken at the indicated time points. Only sporulating hyphae will attach to the hydrophobic cover glass surface. Insets show magnified regions of the colony surface containing spores and spore chains. Bars, 50 μm .

f. Quantification of sporulation shown in (e) via counts of colony-forming units (c.f.u.). The graph shows a 6-fold higher c.f.u. count at 72 h in the $\Delta cisA$ mutant. Strains were grown on R2YE agar and spores were harvested after 48 h, 72 h, and 96 h of incubation. Data show mean \pm s.d. obtained from biological triplicate experiments.

production (**Supplementary Fig. 8**). Our data therefore support the conclusion that the cellular function of CIS^{Sc} in *S. coelicolor* depends on CisA, and its absence impacts the timely cellular and chemical differentiation of *S. coelicolor* hyphae.

Discussion

Here, we identify CisA as an essential membrane-associated factor that mediates the cellular function of CIS^{Sc} particles in *Streptomyces coelicolor*. In the absence of CisA, CIS^{Sc} are not able to contract in the cellular context (**Fig. 1**). Similar to a CIS^{Sc} deletion or non-contractile mutant (18), this decreases the induction of cell death upon stress, which in turn affects cellular development and secondary metabolite production (**Fig. 5**). The mechanistic aspects of this distinct mode of action of a CIS are discussed below.

A conserved feature of all previously studied CIS is the requirement of the contractile apparatus to bind to a membrane before firing. This can be achieved in different ways, leading to the classification of CIS into different modes of action. First, T6SS are anchored to the cytoplasmic membrane of the host cell by a trans-envelope complex spanning from the cytoplasm to the inner membrane, periplasm, and outer membrane (34–36). Second, contractile phages and eCIS bind to the surface of their target cell via tail fibers, which are typically connected to the baseplate and transmit the signal for firing to the baseplate (13,16,37). Third, tCIS are anchored to thylakoid membrane stacks in cyanobacteria by an extension of their baseplate (38). Finally, and in contrast to the previously described CIS, we show that intracellular CIS^{Sc} particles from *Streptomyces* do not include structural components that can directly bind the host membrane. Our data suggest that CisA may be required to mediate an interaction of CIS^{Sc} with the cytoplasmic membrane prior to firing (**Fig. 5**). This interaction may occur directly via the binding of the CIS^{Sc} particle to the membrane protein CisA, or through the interaction with a yet unknown factor. To explore this idea, we performed an *in silico* prediction of protein-protein interactions between monomeric CisA and CIS^{Sc} components using AlphaFold2-Multimer (39) (**Supplementary Fig. 9a**). Interestingly, this analysis identified the baseplate component Cis11 as a significant hit and possible interaction partner of CisA (**Supplementary Fig. 9b-d**). Importantly, such a protein-protein interaction would be consistent with our cryoEM structure (**Fig. 2b-f**), showing a peripheral surface-exposed position of Cis11 in the baseplate complex of extended CIS^{Sc}.

Additional structural modelling using AlphaFold2-Multimer with truncated versions of CisA in complex with Cis11 further support the idea that the largely unstructured cytosolic portion of CisA is required to interact with the Cis11 (**Supplementary Fig. 10**). We have been unable to confirm a direct interaction between CisA and Cis11 because the expression of *cisA* is toxic in *E. coli*, which prevented the experimental analysis of the CisA-Cis11 interaction using co-purification approaches and bacterial two-hybrid studies. However, we did detect CisA peptides in crude purifications of CIS^{Sc} from nisin-stressed cells (Supplementary Table 2). This would be consistent with a transient and/or short-lived interaction of CIS^{Sc} particles with CisA, triggered by an exogenous or cellular signal. In agreement with this idea, we rarely observed extended CIS^{Sc} assemblies associated with the cytoplasmic membrane via their baseplate in WT cells (**Fig. 1d**).

We further speculate that CisA may not only serve as a mediator for the interaction of CIS^{Sc} with the cytoplasmic membrane but also as a sensor and checkpoint for inducing cell death only under specific stress conditions or in response to cellular signals. The CisA C-terminal IgG-like domain that is localized outside the cytoplasm and in proximity of the Gram-positive cell wall may sense stress signals that could potentially trigger conformational changes in CisA, which in turn could mediate the recruitment of CIS^{Sc} assemblies to the cytoplasmic membrane, followed by firing. The fatal outcome of firing for the producing cell may have driven the evolution of a stepwise

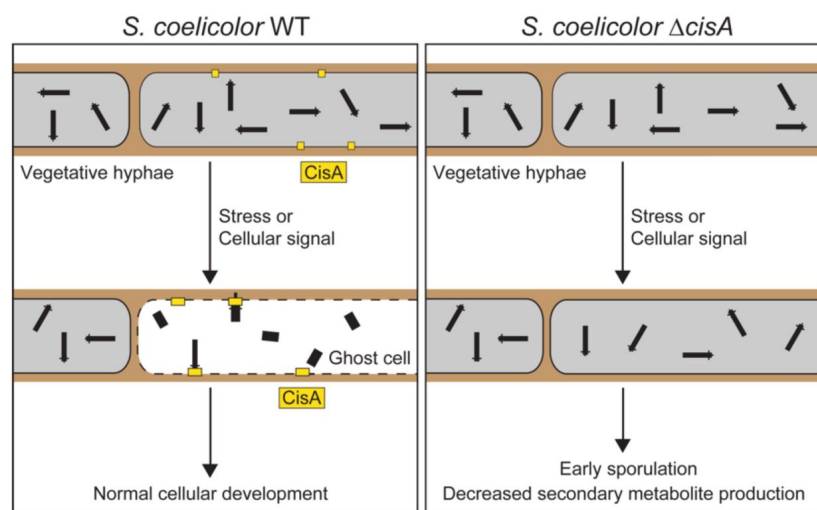


Figure 5

Cytoplasmic CIS^{Sc} require the membrane protein CisA for contraction and function.

Proposed model illustrating a possible role of CisA. In response to exogenous stress or an unknown cellular signal, membrane-bound CisA either directly or indirectly mediates the association of free-floating CIS^{Sc} particles with the cytoplasmic membrane, leading to CIS^{Sc} firing and regulated cell death, which impacts the *Streptomyces* developmental life cycle.

mechanism involving a checkpoint that prevents self-inflicted cell death by accidental firing. Such a mechanism would keep the CIS^{Sc} in a free-floating, non-functional and safe state in the cytoplasm.

Methods

Bacterial strains, plasmids, and oligonucleotides

Bacterial strains, plasmids, and oligonucleotides used in this study are listed in Supplementary Tables 3-4. Plasmids were generated using either standard restriction-ligation or assembled using the Gibson Assembly Master Mix (NEB) or *In Vivo* Assembly. All plasmids were verified by DNA sequencing. *Escherichia coli* strains were cultured in LB, SOB, or DNA medium. *E. coli* strains TOP10, DH5α and NEB5α were used to propagate plasmids and cosmids, *E. coli* strain BW25113/pIJ790 for recombineering cosmids and *E. coli* ET12567/pUZ8002 for interspecies conjugation. When required, media was supplemented with antibiotics at the following concentrations: 100 µg/ml carbenicillin, 50 µg/ml apramycin, 50 µg/ml kanamycin, 50 µg/ml hygromycin.

Streptomyces coelicolor strains were cultivated in LB, TSB, TSB-YEME, or R2YE liquid medium at 30 °C in baffled flasks or flasks with springs, at 250 rpm or grown on LB, SFM, R2YE medium solidified with 1.5 % (w/v) Difco agar (40 [40](#)). Antibiotics were added at the following concentrations: 25 µg/ml apramycin, 50 µg/ml kanamycin, 25 µg/ml hygromycin, 12.5 µg/ml nalidixic acid.

Construction of the *S. coelicolor* Δ*cisA* mutant

The λ RED homologous recombination system was used to isolate gene replacement mutations using PCR-directed mutagenesis (ReDirect) of the *S. coelicolor* cosmid StD8A containing the *cis* gene cluster(41 [41](#)),(42 [42](#)). The *cisA* coding sequence (SCO4242) was replaced with the *aac3(IV)-oriT* resistance cassette from pIJ773. The mutant cosmid (pSS684) was introduced into *E. coli* ET12567/pUZ8002, followed by conjugation into *S. coelicolor* M145. Exconjugants that had successfully undergone double-homologous recombination were identified by screening for apramycin resistance and kanamycin sensitivity. The deletion of *cisA* was subsequently verified by PCR.

Sheath preparation of CIS^{Sc}

S. coelicolor strains were grown in 30 ml TSB, TSB-YEME or R2YE liquid medium for 48 h. Cells were pelleted by centrifugation (7,000 × g, 10 min, 4 °C), resuspended in 5 ml lysis buffer (150 mM NaCl, 50 mM Tris-HCl, 0.5× CellLytic B (Sigma-Aldrich), 1 % Triton X 100, 200 µg/ml lysozyme, 50 µg/ml DNase I, pH 7.4), and incubated for 1 h at 37 °C. Cell debris was removed by centrifugation (15,000 × g, 15 min, 4 °C) and cleared lysates were subjected to ultra-centrifugation (150,000 × g, 1 h, 4 °C). Pellets were resuspended in 150 µl resuspension buffer (150 mM NaCl, 50 mM Tris-HCl, supplemented with protease inhibitor cocktail [Roche], pH 7.4). CIS^{Sc} sheath preparations were analyzed by negative stain EM imaging (43 [43](#)) and mass spectrometry at the Functional Genomics Center Zürich.

To purify non-contractile CIS^{Sc} particles from *S. coelicolor* (SS393), cleared cell lysates were subjected to ultracentrifugation using a sucrose cushion (20 mM Tris pH 8.0, 150 mM NaCl, 50 mM EDTA, 1 % Triton X 100, 50 % [w/v] sucrose) (18 [18](#)). The sucrose cushion alongside 1 mm of liquid above and residual bacterial contaminants were removed by centrifugation at 15,000 × g. Samples were then subjected to a second round of ultracentrifugation without a sucrose cushion (150,000 × g, 1 h, 4 °C) and resulting cell pellets were resuspended in buffer (50 mM Tris, 150 mM NaCl). These crude samples were then purified further by gradient ultracentrifugation (10 %-50 % continuous

gradient made with BIOCOMP gradient master IP model 107 gradient forming instrument) at 100,000 $\times g$ for 1 h using a SW55 Ti rotor. The gradient was analyzed in 11 fractions of 500 μ l and checked by negative stain EM. The fractions, which contained CIS^{Sc} particles, were pooled and used for further experiments.

Negative stain electron microscopy

4 μ l of purified CIS^{Sc} sheath particles were adsorbed to glow-discharged, carbon-coated copper grids (Electron Microscopy Sciences) for 60 s, washed twice with milli-Q water and stained with 2 % phosphotungstic acid for 45 s. The grids were imaged at room temperature using a Thermo Fisher Scientific Morgagni transmission electron microscope (TEM) operated at 80 kV.

Mass spectrometry analysis

To confirm the presence of predicted CIS^{Sc} components, isolated sheath particles were subjected to liquid chromatography–mass spectrometry analysis (LC–MS/MS). These experiments were conducted at the Functional Genomics Center Zürich. First, the samples were digested with 5 μ l of trypsin (100 ng/ μ l in 10 mM HCl) and microwaved for 30 min at 60 °C. The samples were then dried, dissolved in 20 μ l ddH₂O with 0.1 % formic acid, diluted in 1:10 and transferred to autosampler vials for liquid chromatography with tandem mass spectrometry analysis. A total of 1 μ l was injected on a nanoAcquity UPLC coupled to a Q-Exactive mass spectrometer (ThermoFisher). Database searches were performed by using the Mascot swissprot and tremble_streptomycetes search programs. For search results, stringent settings have been applied in Scaffold (1 % protein false discovery rate, a minimum of two peptides per protein, 0.1 % peptide false discovery rate). The results were visualized by Scaffold software ([Proteome Software Inc.], Version 4.11.1).

Protein gel electrophoresis and western blotting

For general protein analysis, protein samples were boiled at 95 °C for 5 min and separated by a 4–20% Mini-PROTEAN® TGX Stain-Free™ SDS PAGE (BioRad) or 12 % Tris-Glycine SDS PAGE (Invitrogen) and visualized using InstantBlue Coomassie Protein Stain or ReadyBlue Protein Gel Stain (Sigma Aldrich).

For western blotting, cells were grown in biological triplicate for 48 h in TSB, 2 ml aliquots of each culture were pelleted and washed once with 1x PBS. Cell pellets were resuspended in 0.4 ml of sonication buffer (20 mM Tris pH 8.0, 5 mM EDTA, 1x EDTA-free protease inhibitors [Sigma Aldrich]) and subjected to sonication at 4.5-micron amplitude for 7 cycles of 15 s on / 15 s off. Samples were centrifuged at 17,000 $\times g$ for 15 min at 4 °C. Protein concentration in cleared cell lysate supernatants was determined by Bradford Assay (Biorad). Equivalent total protein concentrations (1 mg/ml) were assayed using the semi-dry western blot transfer. The gel was transferred to a PVDF membrane (Biorad) and probed with the appropriate antibody diluted in TBS-T or using the iBIND buffer system (Thermo Fisher): Rabbit anti-FLAG ([Sigma Aldrich] F7425, 1:2500), Rabbit anti-WhiA ((44 [DOI](#)), 1:2500), and Goat Anti-Rabbit-HRP (Abcam Ab6721, 1:5000). To visualize HRP-conjugated antibodies, membranes were incubated with SuperSignal West Femto ECL solution (Thermo Fisher).

Cellular fractionation

To fractionate membrane and soluble proteins from *S. coelicolor* (WT, SS576), cells were grown for 48 h in 50 ml TSB/YEME and harvested by centrifugation. Cell pellets were resuspended in 1/10 volume of lysis buffer (0.2 M Tris-HCl, pH 8, 10 mg/mL lysozyme, and 1x EDTA-free protease inhibitors; [Roche]), incubated for 30 min at 37 °C, and then briefly cooled on ice before lysed by sonication (11 x 15 sec on/off at 50 % power at 8 microns on ice). Cell debris was removed by centrifugation at 16,000 $\times g$ for 20 min and supernatant was subsequently subjected to two additional rounds of centrifugation. The cleared cell lysate was subjected to ultracentrifugation for

1 h at $150,000 \times g$ at 4 °C to separate the soluble proteins from membrane proteins. Sedimented membrane proteins were resuspended and washed twice in 1 volume of wash buffer (60 mM Tris-HCl, 200 mM NaCl, pH 8, 0.2 mM EDTA, and 0.2 M sucrose) at $150,000 \times g$ at 4 °C for 1 h. The wash step was repeated one final time with the wash buffer containing 8 M urea to remove traces of membrane-associated proteins (45). The final pellet was dissolved in 1/10 of the initial volume with wash buffer (no urea). Equi-volume amounts of fractions were mixed with 2x SDS sample buffer and analyzed by immunoblotting.

Membrane protein topology analysis in *E. coli*

The coding sequence of CisA was inserted in the dual pho-lac reporter plasmid pKTop, which consists of an *E. coli* alkaline phosphatase fragment PhoA₂₂₋₄₇₂ fused in frame after the α -fragment of β -galactosidase LacZ₄₋₆₀ (Supplementary Table 3) (29). For membrane protein topology, *E. coli* TG1 was transformed with the pKTop and derivatives. Membrane protein topology was assayed by plating the resulting reporter strains on dual-indicator plates containing LB agar supplemented with 80 μ g/ml 5-bromo-4-chloro-3-indolyl phosphate disodium salt (X-Phos) ([Sigma Aldrich], RES1364C-A101X) and 100 μ g/mL 6-chloro-3-indolyl- β -d-galactoside (Red-Gal) ([Sigma Aldrich], B6149) as indicators, 1 mM IPTG, and 50 μ g/ml kanamycin. A periplasmic or extracellular location of the reporter fusion results in higher alkaline phosphatase activity (blue color), whereas a cytosolic location of the reporter leads to higher β -galactosidase activity (magenta color). Plates were incubated for two days at 37 °C and scanned.

Vitrified sample preparations

For single-particle cryoEM (SPA), the *S. coelicolor* non-contractile CIS particles were purified as described above and vitrified using a Vitrobot Mark IV (Thermo Fisher Scientific). 4 μ l of samples were applied twice on glow-discharged 200 mesh Quantifoil copper grids (R 2/2) which were manually coated with a layer of 1 nm carbon. Grids were blotted for 5.5 s and plunge-frozen in liquid ethane-propane mix (37 %/63 %). Frozen grids were stored in liquid nitrogen until loading into the microscope.

For cryo-electron tomography (cryoET), *Streptomyces* cells were mixed with 10 nm Protein A conjugated colloidal gold particles (1:10 v/v, [Cytodiagnostics]) and 4 μ l of the mixture was applied to a glow-discharged holey-carbon copper EM grid (R2/1 or R2/2, [Quantifoil]). The grid was automatically blotted from the backside for 4-6 s in a Mark IV Vitrobot by using a Teflon sheet on the front pad, and plunge-frozen in a liquid ethane-propane mixture (37 %/63 %) cooled by a liquid nitrogen bath.

SPA data collection and image processing

44,925 movies were collected on Titan Krios microscope (Thermo Fisher Scientific), operated at 300 keV equipped with K3 direct electron detector, operating in counting mode, and using a slit width of 20 eV on a GIF-Quantum energy filter (Gatan). The automated data collection was conducted with EPU software (Thermo Fisher Scientific) with a final pixel size of 1.065 Å/pix over 40 frames with a total dose of 50 e⁻/Å². The targeted defocus was set between -1.6 and -2.8 μ m with 0.2 μ m increment.

Movie-alignments with dose-weighting were performed in MotionCor2 software (46) with a gain reference estimated a posteriori (47) followed by standard in-house pipeline of manual inspection and selection of 38,845 micrographs (48) for further processing in cryoSPARC package v4.0.3 (49). Due to the low concentration of particles and the presence of other contaminants in the sample, automatic particle picking appeared challenging, and we developed CIS-specific approach for efficient picking of the cap and baseplates. In this approach, CIS^{Sc} particles were manually selected as filaments (start-to-end) on 920 micrographs and used for training a crYOLO (50) picking model (Supplementary Fig. 2). The large size of the training

set appeared essential for successful picking; we could not get rid of large number of false-positive picks, but there were not so many false-negative picks. Then, CIS^{Sc} particles were picked in crYOLO as filaments, followed by the extraction of the ends of the “filaments” using star_modif.py script (48 [48](#)). Particle coordinates were imported in cryoSPARC, where 211,041 particles were extracted at a large box size of 756 pixels binned to 64 pixels for initial 2D-classification, which allowed us to separate initial particle sets corresponding to the CIS^{Sc} cap (36,569 particles) and CIS^{Sc} baseplate (43,087 particles) (**Supplementary Fig. 2** [49](#)).

Two subsets of this dataset were processed in cryoSPARC separately. For the cap subset, a standard cryoSPARC single-particle processing approach was applied, including gradual iterative 2D-classification rounds, followed by selection of good classes and particle re-extraction at finer sampling. The main challenge was the proper centering of the particles selected on the end of elongated filament-like objects with repeating patterns (sheath-tube module of CIS), hampering the alignments. Ab-initio model generation with applied C6 symmetry was hampered by poor centering of 2D-classes due to elongated nature of the particles (**Supplementary Fig. 2** [49](#)). Homo-refinement with this reference was performed followed by particle re-extraction and one more round of ab-initio model generation with applied C6 symmetry (**Supplementary Fig. 2** [49](#)). The new 3D-reconstruction appeared reliable and was used for further iterative 3D-refinements (Homo-refinement and NU-refinements) accompanied by 2D-classification and CTF-refinement rounds to exclude particles with wrong Euler angle assignments. The final 3.4 Å resolution map with imposed C6 symmetry resulted from 19,218 particles.

The baseplate subset was processed using the same approach, resulting in a 3D-reconstruction with imposed C6 symmetry with a resolution of 3.5 Å from 22,980 particles (**Supplementary Fig. 2** [49](#)). The tip of the baseplate has a C3 symmetry, therefore to solve that part of the map correctly, we exported that particle stack to Relion4 (51 [51](#)) and took advantage of 2D-classification in Relion to select 18,124 particles, corresponding to the best 2D classes averages. 3D-refinement with relaxed symmetry resulted in a 3.8 Å 3D-resolution reconstruction with imposed C3 symmetry.

Cryo-electron tomography

Intact *Streptomyces* cells were imaged by cryoET as described previously (52 [52](#)). Images were recorded using a Titan Krios 300 kV microscope (Thermo Fisher Scientific) equipped with a Quantum LS imaging filter operated at a 20 eV slit width and with K3 Summit direct electron detectors (Gatan). Tilt series were collected using a bidirectional tilt-scheme from -60 to +60° in 2° increments. Total dose was 130-150 e-/Å² and defocus was kept at -8 µm. Tilt series were acquired using SerialEM (53 [53](#)), drift-corrected using alignframes, and reconstructed using IMOD program suite (54 [54](#)). To enhance contrast, tomograms were deconvolved with a Wiener-like filter ‘tom_deconv’ (55 [55](#)).

Structural modeling of the CIS^{Sc} complex

The map qualities of different modules of CIS^{Sc} (cap and baseplate) allowed for *de novo* structural modelling (**Supplementary Fig. 2** [49](#)-[3](#) [49](#)). The atomic models of SCO4243-4248, SCO4252-4253 and SCO4260 were built *de novo* using COOT (56 [56](#)). The resulting models were iteratively refined using RosettaCM (57 [57](#)) and real-space refinement implemented in PHENIX (58 [58](#)). In cases where protein domains could only be partially modeled, side chains were not assigned. Final model validation was done using MolProbity (58 [58](#)) and correlation between models and the corresponding maps were estimated using mtriage (58 [58](#)). To illustrate the complete CIS^{Sc} structure, we generated a composite model by integrating symmetry-related protein subunits into a full model of the CIS^{Sc}, based on the consistent CIS^{Sc} length observed both *in situ* and *in vitro* (**Fig. 2b** [49](#)).

Fluorescence microscopy

Fluorescence-based cell viability assays were performed as described previously (18). Briefly, to produce cytoplasmic sfGFP in *Streptomyces*, the coding sequence for sfGFP was introduced downstream of the constitutive promoter *ermE** on an integrating plasmid. The plasmid was introduced by conjugation to *S. coelicolor* strains (SS430, SS575, SS576). An equal level of cytoplasmic sfGFP in the different strains was confirmed by Western blotting (Supplementary Fig. 11). *Streptomyces* strains were grown in 30 ml of TSB liquid culture at 30 °C with shaking at 250 rpm for 48 h. Where appropriate, nisin was added to a final concentration of 1 µg/ml 90 min prior to imaging. One ml aliquots of each culture were centrifuged for 5 min at 15,000 x g, washed twice with 1xPBS, resuspended in 1 ml of 1xPBS containing 5 µg/ml of the red-fluorescent membrane dye FM5-95 (Invitrogen) and then incubated in the dark at room temperature for 10 min followed by two wash steps with 1x PBS. Washed cell pellets were resuspended in a total volume of 50 µl PBS and 10 µl of each sample was spotted onto 1 % agar pads and subsequently imaged using the Thunder imager 3D cell culture microscope (Leica). First, tile scan images were acquired using the Las X Navigator plug-in software (Leica Application Suite X, Version 3.7.4.23463), and 100 regions of interest were picked manually. Then Z-stack images were acquired using a HC PL APO 100x objective with the following excitation wavelengths: GFP (475 nm) and TRX (555 nm). Images were processed using LasX software to apply thunder processing and maximum projection and FIJI to create segmentation and quantify the live (sfGFP)/total cells (FM5-95) area ratio (59). Statistical analyses were performed on data from biological triplicates (n=100 images for each experiment) using a one-way ANOVA and Tukey's post-test in GraphPad Prism 9 (Version 9.3.1).

For imaging the subcellular localization of the CIS adaptor protein in *Streptomyces*, cells (strain JS69 or *S. coelicolor* M145) were grown for 48 h in TSB/YEME liquid medium. Two µl of each strain were spotted on 1 % agarose pads and subsequently imaged. Images were acquired using a Zeiss Axio Observer Z.1 inverted epifluorescence microscope fitted with a sCMOS camera (Hamamatsu Orca FLASH 4), a Zeiss Colibri 7 LED light source, and a Hamamatsu Orca Flash 4.0v3 sCMOS camera. mCherry fluorescence was detected using an excitation/emission bandwidth of 577–603 nm/614–659 nm. Images were collected using Zen Blue (Zeiss) and analyzed using Fiji (59).

Cover glass impression of *Streptomyces* spore chains

Spore titers of relevant strains were determined by dilution plating (18). 10^7 colony forming units (CFU) of *S. coelicolor* strains (WT, SS539, SS557) were spread onto R2YE agar plates and grown at 30 °C. Sterile glass coverslips were gently applied to the top surface of each bacterial lawn after 48 h, 72 h and 96 h post inoculation. Coverslips were then mounted onto glass microscope slides and imaged using a 40x objective on a Leica Thunder Imager 3D Cell Culture. Images were processed using FIJI (59).

Actinorhodin production assay

S. coelicolor strains (WT, SS539, SS557) were inoculated into 30 ml R2YE liquid media at a final concentration of 1.5×10^6 CFU/ml. Cultures were grown in baffled flasks at 30 °C overnight. Cultures were standardized to an OD₄₅₀ of 0.5 and inoculated in 30 ml of fresh R2YE liquid medium. For visual comparison of pigment production, images of the growing culture were taken between t = 0 and t = 72 h (as indicated in Supplementary Fig. 7). For quantification of total actinorhodin production, 480 µl of samples were collected at the same time points where images were taken. 120 µl of 5M KOH was added, samples were vortexed and centrifuged at 5,000 x g for 5 min. The weight of each tube was recorded. A Synergy 2 plate reader (Biotek) was used then to measure the absorbance of the supernatant at 640 nm. The absorbance was normalized by the weight of the wet pellet.

Structure prediction and in silico protein-protein interaction screen

CisA structure was predicted using AlphaFold2 (28 [↗](#)) and further processed using UCSF Chimera (60 [↗](#)) or ChimeraX-1.7.1 (61 [↗](#)).

A pairwise *in silico* screen for possible interactions between CisA and components encoded by the *S. coelicolor* *cis* gene cluster (*SCO4242-SCO4260*) was conducted using the AlphaFold2 Multimer-based LazyAF pipeline (28 [↗](#), 39 [↗](#), 62 [↗](#)). The confidence metric (ipTM) for the top model from each pairwise interaction was tabulated and visualised using Prism (Version 10.2.2) with ipTM scores >0.7, indicating a possible protein-protein interaction (63 [↗](#)).

Bioinformatic analysis of CisA homologs

To identify CisA homologs, we performed a reciprocal BLAST search in 120 genomes of *Streptomyces* and other *Actinomycete* species that were previously reported to include a type II d eCIS (8 [↗](#), 19 [↗](#)) using the closely related *cisA* homologue from *Streptomyces albus* J1074 (YP_007743954.1) as a query (72% identical to CisA from *S. coelicolor*) (Supplementary Data 1). Of these 120 genomes, 75 had a reciprocal hit for CisA (Supplementary Data 2). Protein sequences of CisA homologs were aligned using Clustal Omega (64 [↗](#)) and visualized with JalView (Version 2.11.3.3).

Data availability

Representative reconstructed tomograms (EMD-50935, EMD-50939, EMD-50940, EMD-50944, EMD-50948, EMD-50949) and SPA cryoEM maps (EMD-51564, EMD-51565 and EMD-51566) have been deposited in the Electron Microscopy Data Bank. Atomic models (PDB: 9GTP, PDB: 9GTR, PDB: 9GTS) have been deposited in the Protein Data Bank.

Acknowledgements

We thank ScopeM for instrument access at ETH Zürich. We thank the Functional Genomics Center Zürich for mass spectrometry support. Pilhofer Lab members are acknowledged for discussions. M.P. was supported by the Swiss National Science Foundation (31003A_179255/310030_212592), the European Research Council (679209), and the NOMIS foundation. Work in the lab of S.S. was supported by a Royal Society University Research Fellowship (URF\R\180075 and URF\R\231009) and BBSRC grant BB/T015349/1 to S.S. and by the BBSRC Institute Strategic Program grant BB/X01097X/1 to the John Innes Centre.

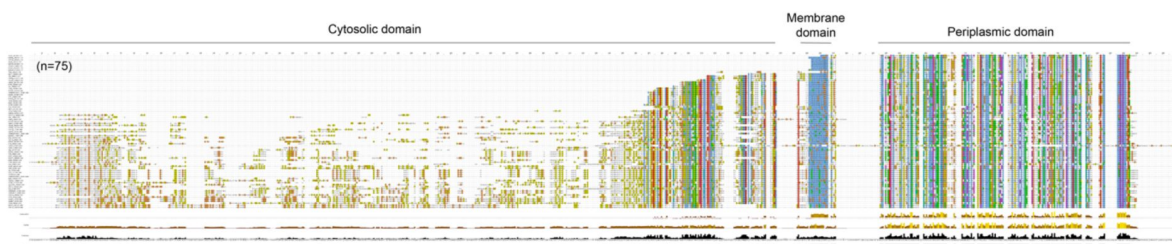
Author contributions statement

B.C., S.S. and M.P. conceived the project. B.C. optimized the sample preparation for SPA; B.C. and P.A. collected and processed the cryoEM data, reconstructed the cryoEM map; B.C., P.E.H. and J.X. built and refined the structural models; B.C. and P.E.H. conducted and processed cryoET; B.C. conducted automated fluorescent light microscopy, determined sporulation efficiency and actinorhodin production; J.W.S. and S.S. generated plasmids and *Streptomyces* strains; J.W.S. designed constructs and performed membrane topology assay. J.W.S. prepared samples and

performed cellular fractionation experiment. J.W.S. imaged strains expressing fluorescently tagged CisA. S.S. and G.C. performed bioinformatic analysis of CisA. B.C., J.W.S., S.S. and M.P. wrote the manuscript.

Competing interests statement

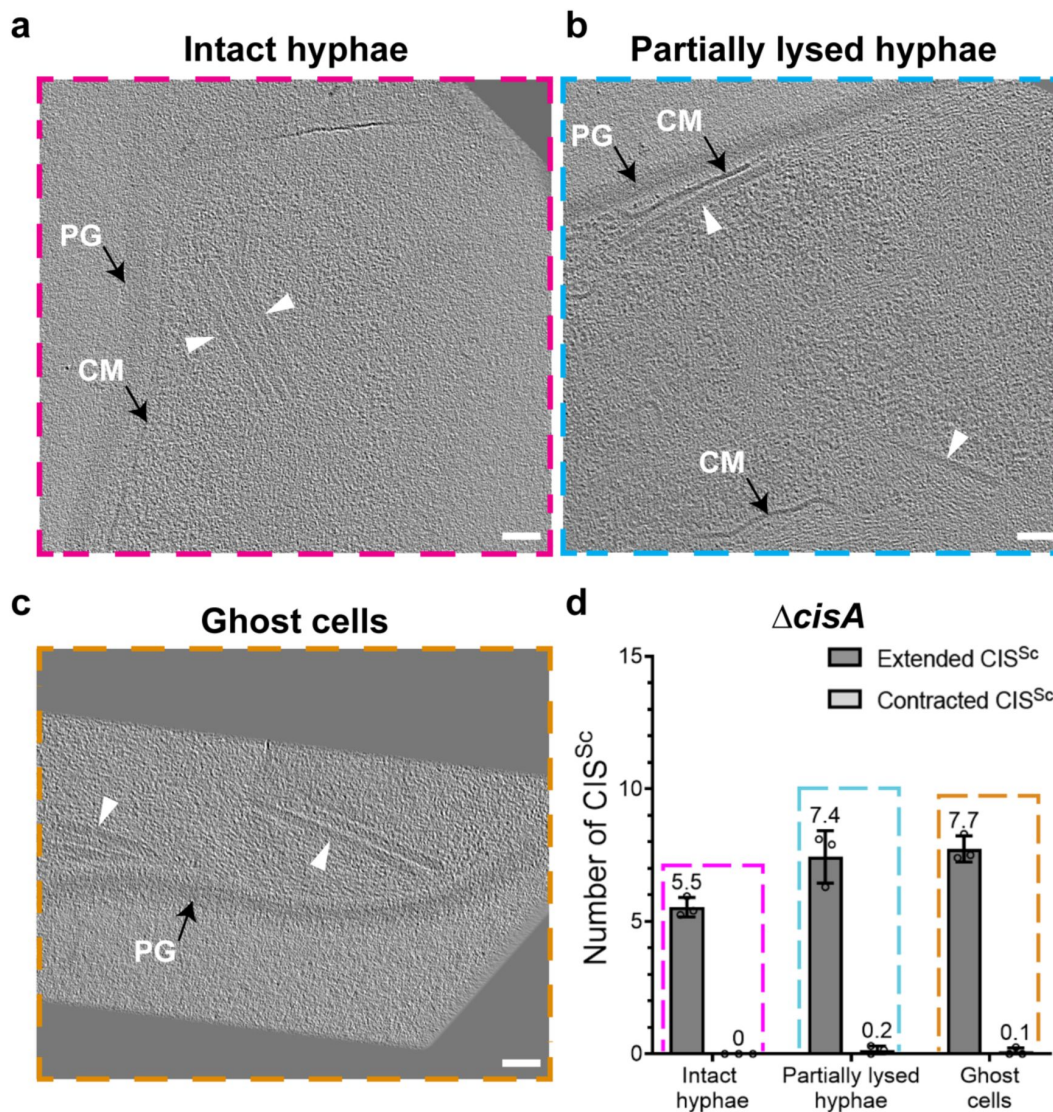
The authors declare no competing interests.



Supplementary Figure 1

CisA is conserved among CIS-positive *Streptomyces* and Actinomycete species.

Protein alignment of CisA homologs identified via reciprocal BLAST search in genomes of *Streptomyces* and Actinomycete species previously reported to encode an eCIS class II_d region. Protein sequences (n=75) were aligned with Clustal Omega and visualized using JalView. CisA domain structure is indicated on top. Genome accession numbers and BLAST results are listed in Supplementary Data 1 and 2.

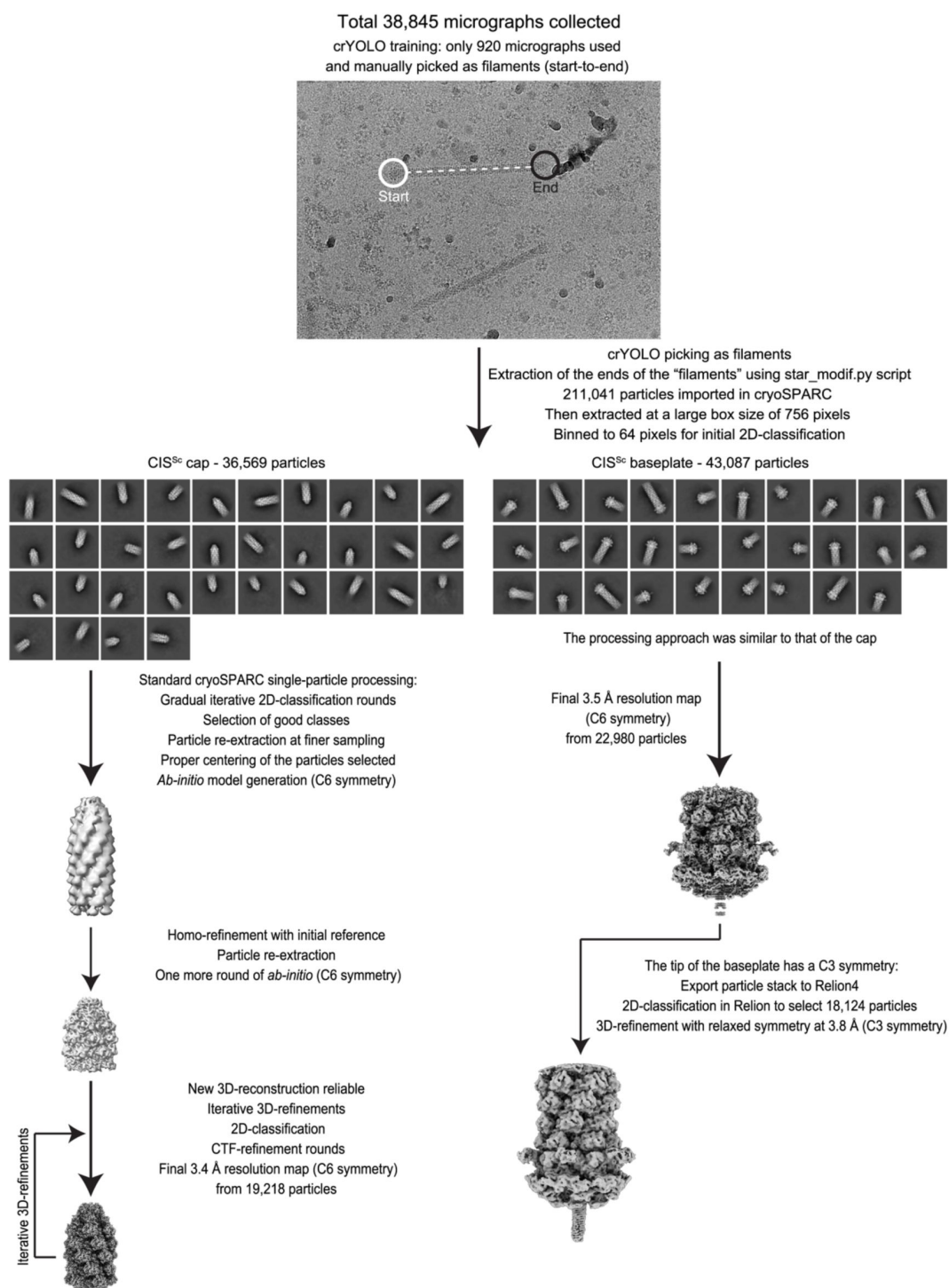


Supplementary Figure 2

Sheath contraction *in situ* is linked to the presence of CisA.

a-c. Shown are additional cryo-tomographic slices (thickness 11 nm) of *S. coelicolor* $\Delta cisA$ vegetative hyphae, which were observed as 'Intact hyphae' (a), 'Partially lysed hyphae' (b) and 'Ghost cells' (c). Note that all visible CIS^{Sc} particles (white arrowheads) are in the extended conformation. PG, peptidoglycan; CM, cytoplasmic membrane/membranes. Bars, 50 nm.

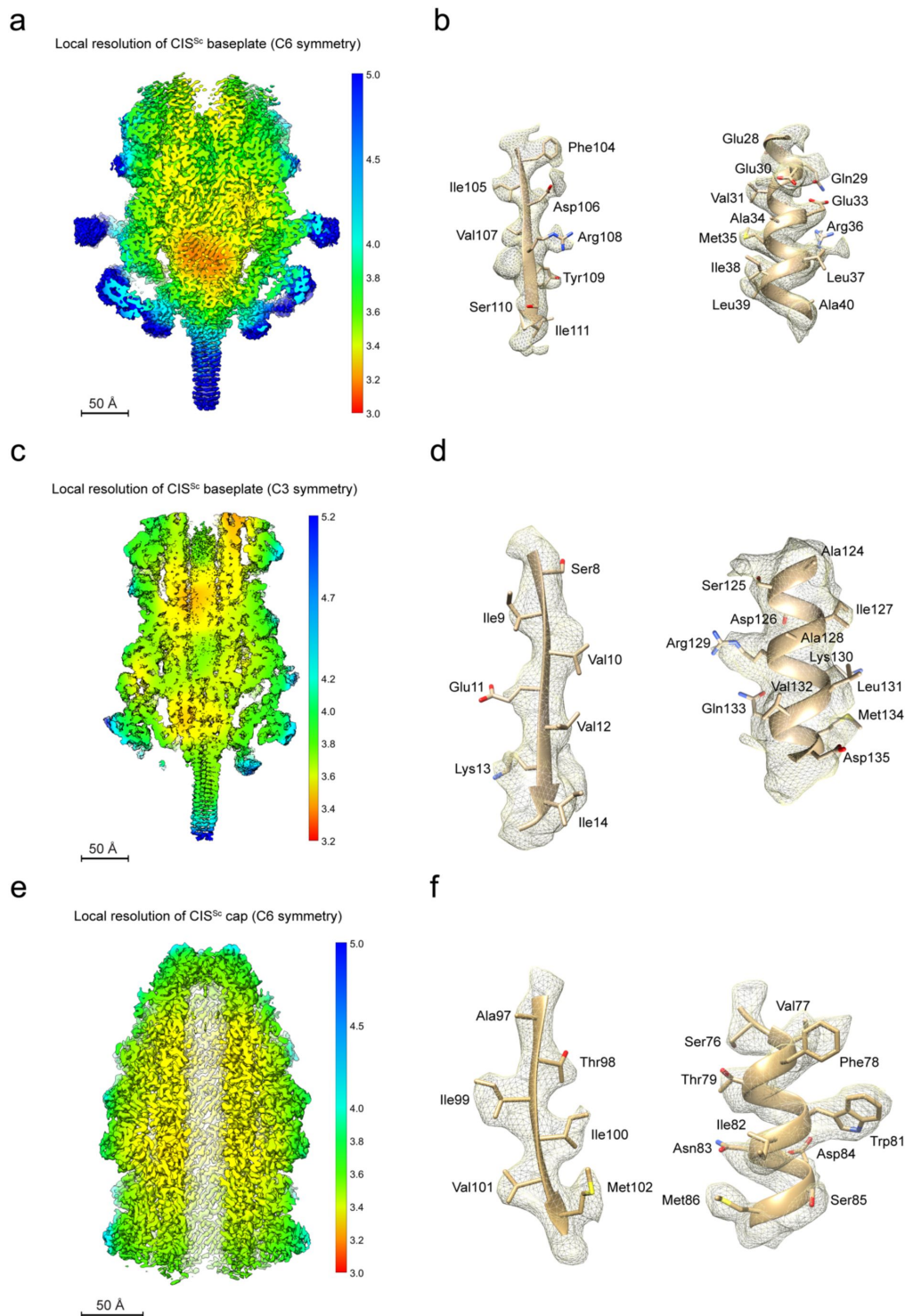
d. Shown is a quantification of CIS^{Sc} assemblies per tomogram and their conformations as observed in different classes of $\Delta cisA$ hyphae. Almost all CIS^{Sc} particles were seen in the extended conformation, indicating that sheath contraction *in situ* correlates with the presence of CisA. Data shows mean values and standard deviations obtained from biological triplicate experiments, with n=30 tomograms for each class of hyphae.



Supplementary Figure 3

Workflow for the cryoEM structural determination of the extended CIS^{Sc}.

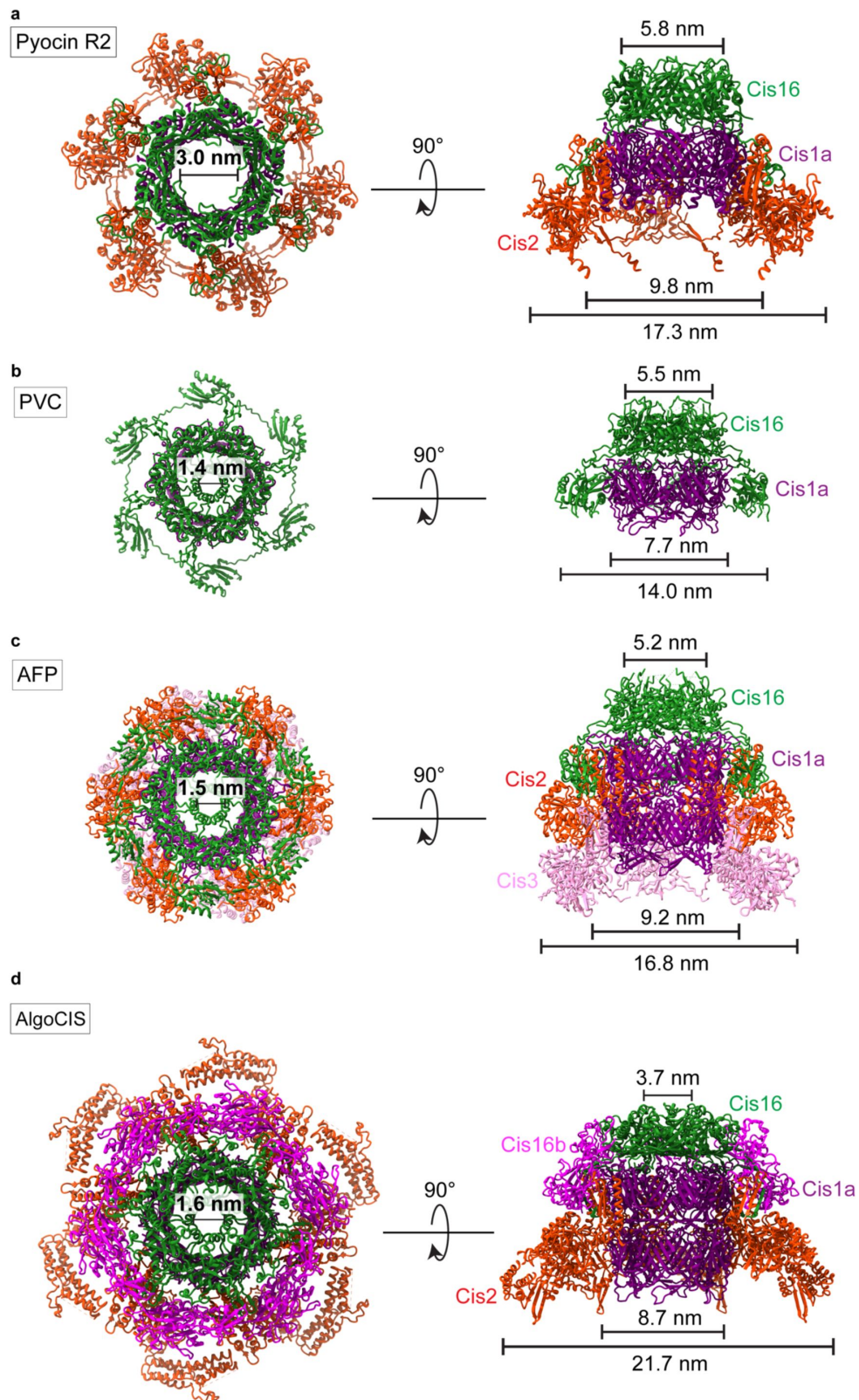
Flowchart for cryoEM reconstruction of the extended CIS^{Sc} particle. See METHODS and Supplementary Table 1 for details.



Supplementary Figure 4

Map qualities of different CIS^{Sc} modules.

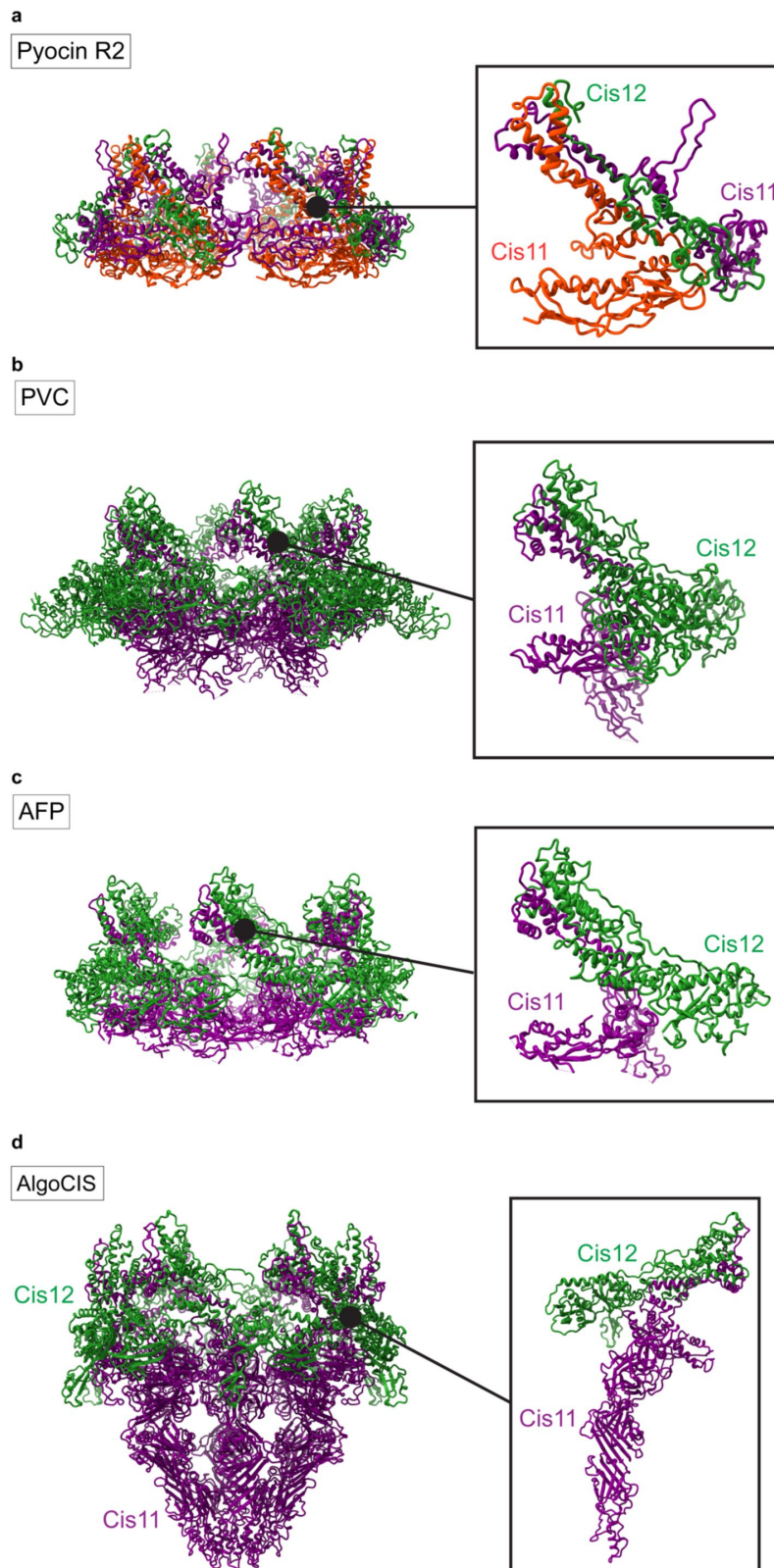
a-f. Local resolution maps of the CIS^{Sc} baseplate with C6 symmetry (a), CIS^{Sc} baseplate with C3 symmetry (c), and the CIS^{Sc} cap with C6 symmetry (e). (d-f) shows regions of the cryoEM density map (mesh) that were superimposed with the atomic models (ribbons and sticks), demonstrating the agreement between the observed and modeled amino acid side chains for one beta-sheet (left) and one alpha helix (right). Shown are examples of the baseplate with C6 symmetry (b), the baseplate with C3 symmetry (d), and the cap with C6 symmetry (f).



Supplementary Figure 5

Structures of the cap modules of other CISs.

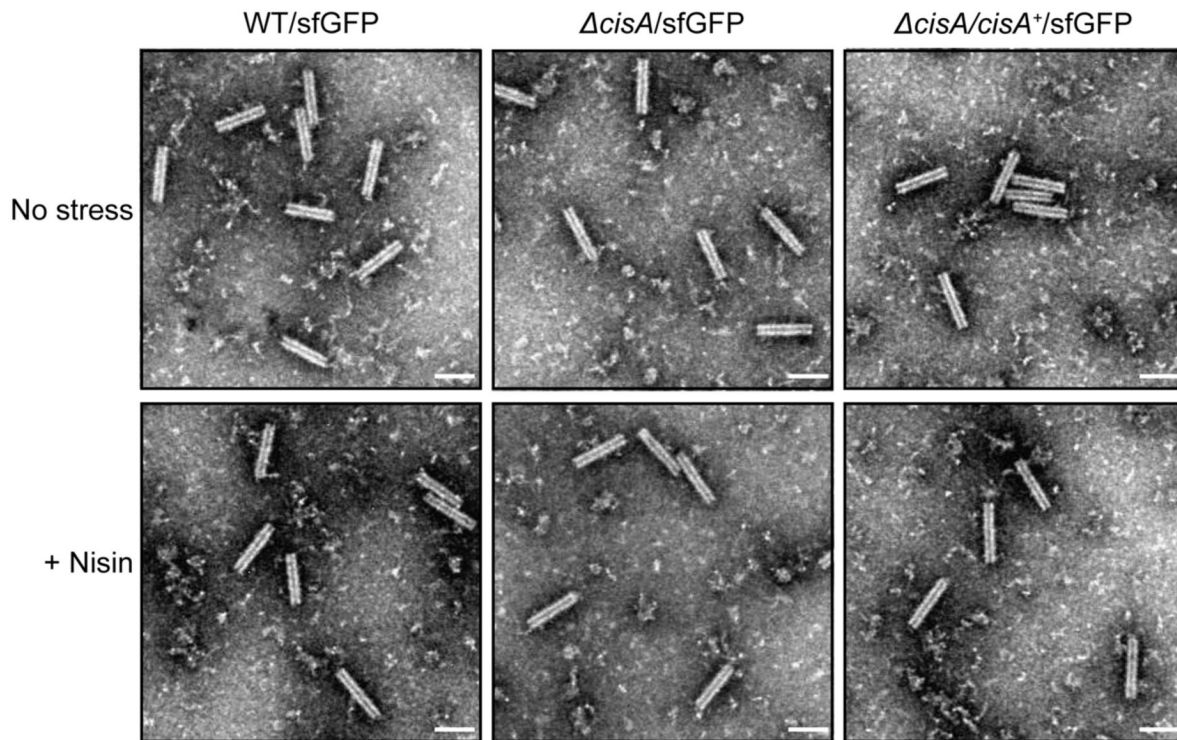
a-d. Top views (left) and side views (right) of ribbon representations of the structures of CIS cap modules of Pyocin R2 (a, PDB 6U5B), PVC (b, PDB 6J0N), AFP (c, PDB 6RAP) and AlgoCIS (d, PDB 7ADZ).



Supplementary Figure 6

Structures of the baseplate modules of other CISs.

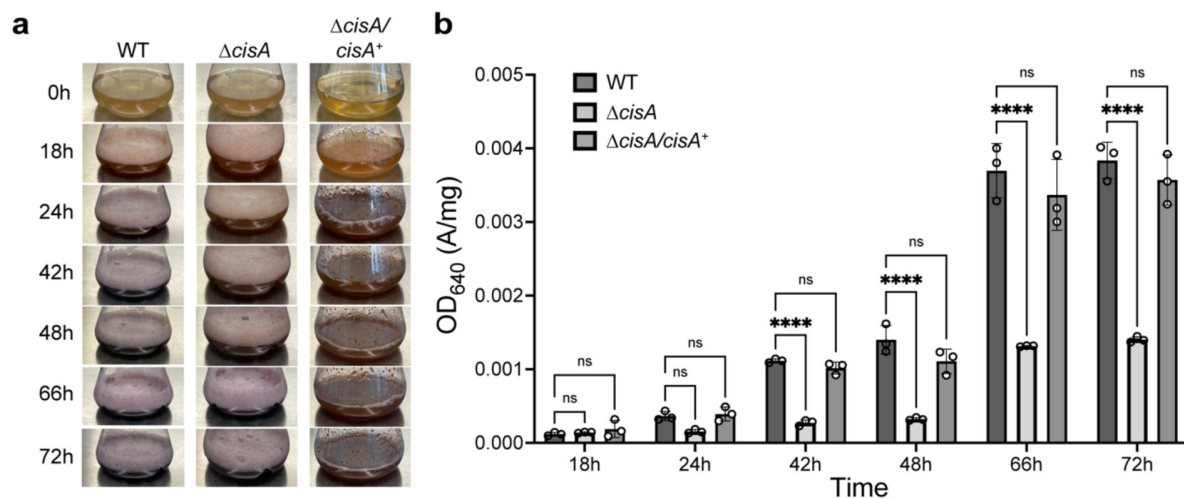
a-d. Ribbon representations of the full structures (left) and the individual wedge subunit (right) of the CIS baseplate components (Cis11/12) of Pyocin R2 (a, PDB 6U5F), PVC (b, PDB 6J0F), AFP (c, PDB 6RAO) and AlgoCIS (d, PDB 7AEB).



Supplementary Figure 7

Control experiment showing that CIS^{Sc} particles are comparable in the strains used in the viability assay.

Representative negative-stain electron micrographs of purified CIS^{Sc} particles from the WT/sfGFP, the $\Delta cisA$ /sfGFP mutant and the $\Delta cisA/\Delta cisA^+$ /sfGFP complemented mutant exposed to no stress (upper row) or 1 μ g/ml nisin (lower row). No differences were observed between the overall structure of CIS^{Sc} particles. These experiments were performed three independent times. Bars, 100 nm.

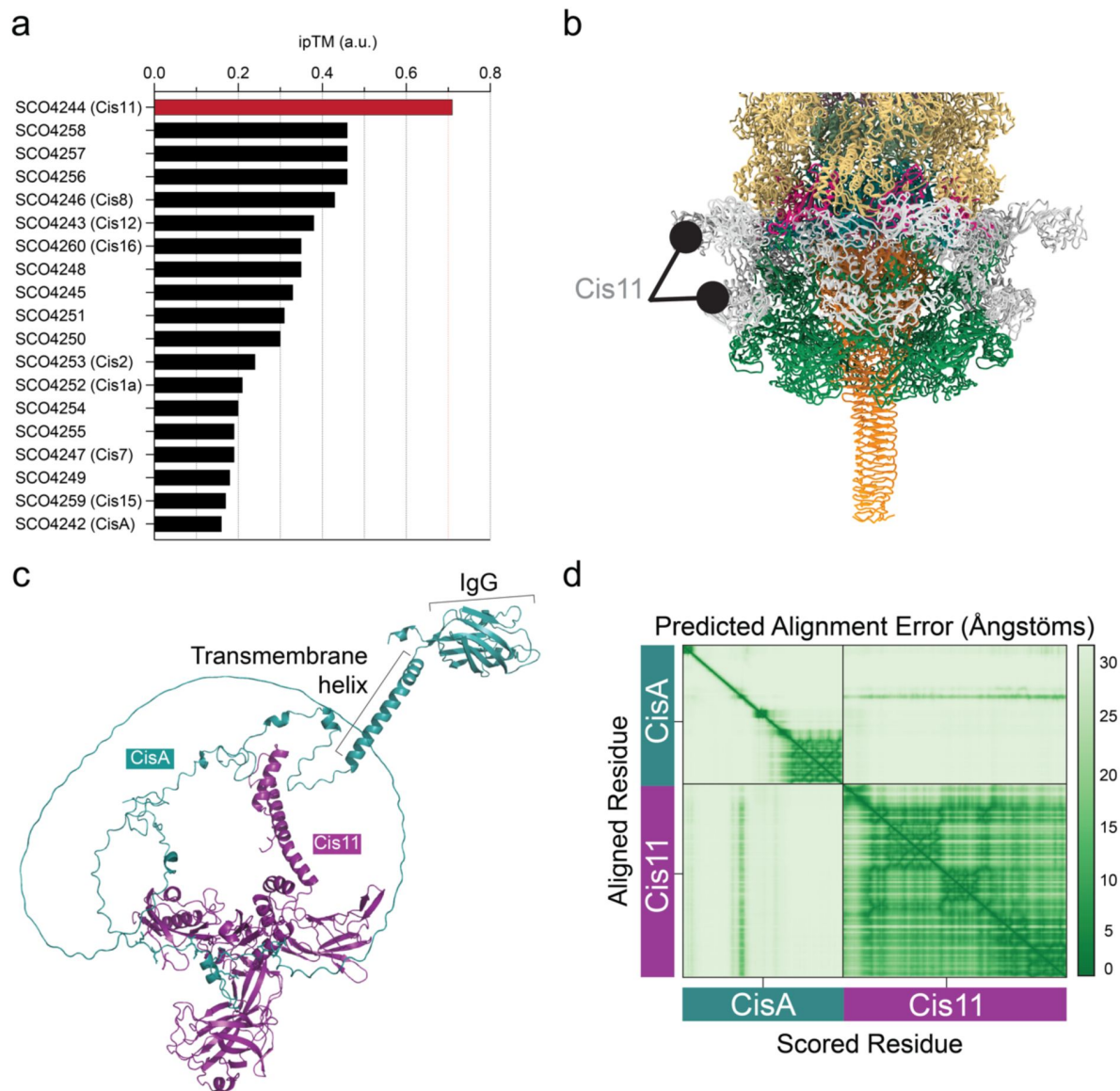


Supplementary Figure 8

CisA impacts secondary metabolite production.

a. Comparison of cultures of WT, $\Delta cisA$ mutant and $\Delta cisA/cisA^+$ mutant in R2YE liquid medium. The coloration of the culture is indicative of actinorhodin (purple) and undecylprodigiosin (red) production (33). Images of each culture flask were taken at the indicated time points.

b. Quantification of total actinorhodin production by the strains shown in (a), revealing reduced production in the $\Delta cisA$ mutant. Samples were taken at the indicated time points. Actinorhodin was extracted and quantified by measuring the optical density OD_{640} of the culture supernatant (65) and normalized to the wet pellet weight. Analysis was performed in biological triplicate experiments. The mean values and standard error are shown. ns (not significant) and **** ($p < 0.0001$) were calculated using one-way ANOVA and Tukey's post-test.



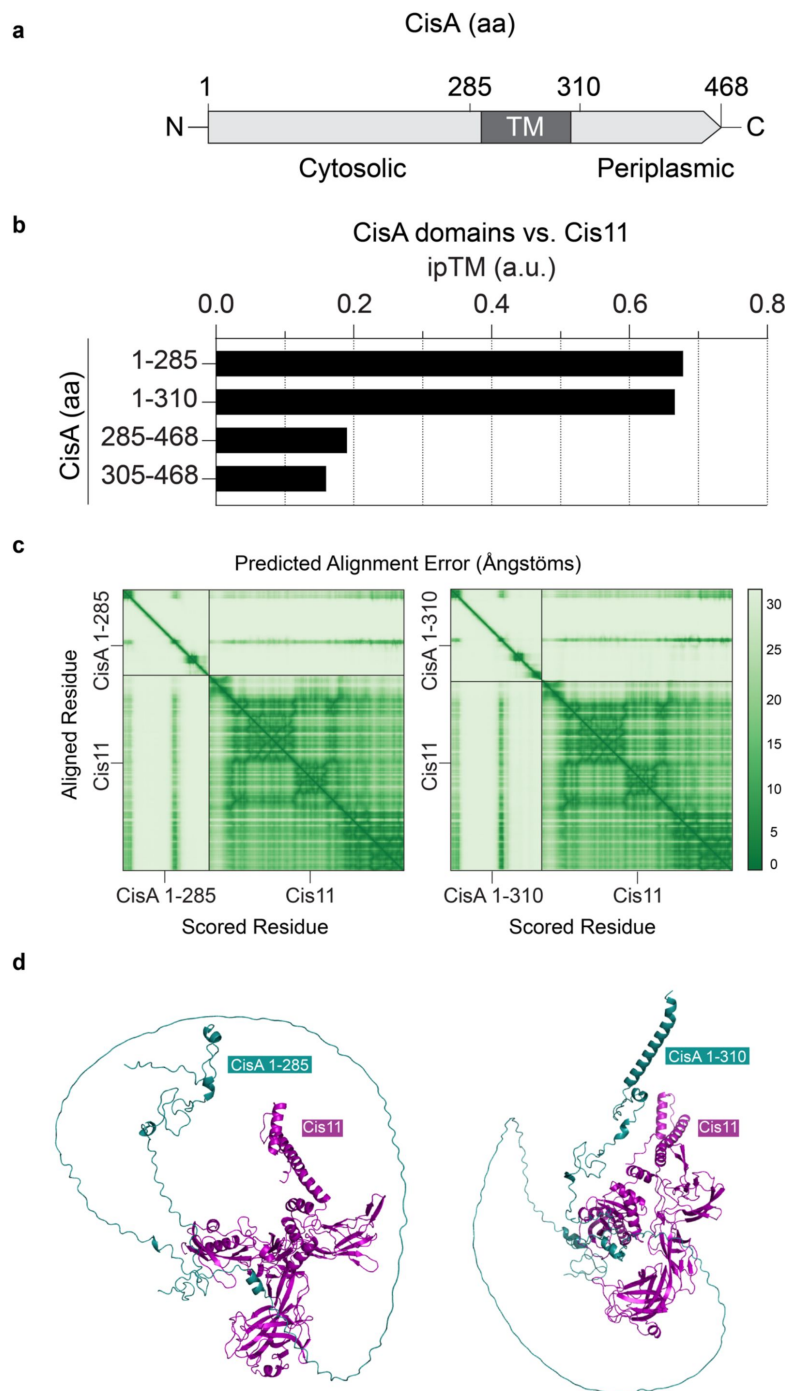
Supplementary Figure 9

***In silico* protein-protein interaction analyses predict that CisA binds a CIS^{Sc} baseplate component.**

a. An AlphaFold2-Multimer-based protein-protein interaction screen between monomeric CisA and the 19 gene products of the CIS^{Sc} gene cluster suggests an interaction between CisA and the baseplate component Cis11. The likelihood of a protein-protein interaction was ranked based on the interface pTM (ipTM) confidence score, with an ipTM greater than 0.7 indicating a potential protein-protein interaction.

b. Zoomed-in view of the SPA-cryoEM structure of the CIS^{Sc} baseplate complex (**Fig. 2b/d**), illustrating the peripheral and surface-exposed position of Cis11.

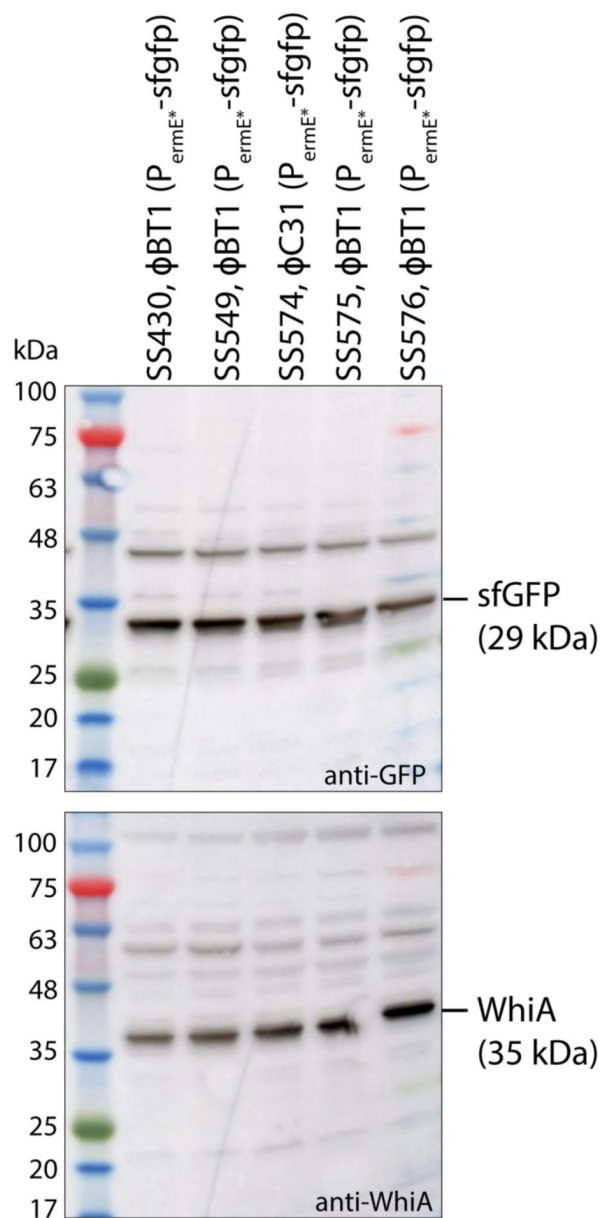
c/d Predicted CisA-Cis11 complex. (c) The AlphaFold3 model of the CisA-Cis11 complex. The “IgG” domain at the C-terminal end of CisA is located in the periplasm. (d) The AlphaFold3 predicted aligned error (%) heatmap plot of the concatenated Cis11 and CisA input sequence.



Supplementary Figure 10

The cytosolic part of CisA is predicted to interact with Cis11.

- a.** Schematic showing the CisA domain organization. Relevant amino acid (aa) positions are shown above. TM, transmembrane domain.
- b.** AlphaFold2-Multimer based protein-protein interaction screen between monomers of CisA and truncated versions of CisA and Cis11. The likelihood of a protein-protein interaction was ranked based on the interface pTM (ipTM) confidence score.
- c/d.** Predicted CisA-Cis11 complexes using truncated versions of CisA (amino acids 1-285 and 1-310) show that the largely unstructured cytosolic portion of CisA is required to interact with Cis11. (c) The AlphaFold3 predicted aligned error (%) heatmap plot of the concatenated Cis11 and truncated CisA 1-285 and CisA 1-310 input sequences. (d) The AlphaFold3 model of the CisA 1-285-Cis11 (left) and CisA 1-310-Cis11 (right) complexes.



Supplementary Figure 11

Western blot confirming similar levels of cytosolic sfGFP in strains used for viability assays.

Control experiments to verify similar protein levels of sfGFP which was expressed either from the ϕ C31 or the ϕ BT1 phage attachment site in the *S. coelicolor* genome. Expression of *sfGFP* was driven from the constitutive *ermE** promoter (P_{ermE^*}). Equal amounts of total protein were loaded and sfGFP levels were detected with an anti-GFP antibody. As a control, the same cell lysates were also probed with an anti-WhiA antibody. Shown are representative results of duplicate experiments.

References

1. Lin L (2024) **The expanding universe of contractile injection systems in bacteria** *Curr Opin Microbiol* **79**
2. Brackmann M, Nazarov S, Wang J, Basler M (2017) **Using Force to Punch Holes: Mechanics of Contractile Nanomachines** *Trends Cell Biol* **27**:623–32
3. Taylor NMI, van Raaij MJ, Leiman PG (2018) **Contractile injection systems of bacteriophages and related systems** *Mol Microbiol* **108**:6–15
4. Taylor NMI, Prokhorov NS, Guerrero-Ferreira RC, Shneider MM, Browning C, Goldie KN, et al. (2016) **Structure of the T4 baseplate and its function in triggering sheath contraction** *Nature* **533**:346–52
5. Böck D, Medeiros JM, Tsao HF, Penz T, Weiss GL, Aistleitner K, et al. (2017) **In situ architecture, function, and evolution of a contractile injection system** *Science* **357**:713–7
6. Allsopp LP, Bernal P (2023) **Killing in the name of: T6SS structure and effector diversity** *Microbiology* **169**
7. Coulthurst S (2019) **The Type VI secretion system: a versatile bacterial weapon** *Microbiol Read Engl* **165**:503–15
8. Chen L, Song N, Liu B, Zhang N, Alikhan NF, Zhou Z, et al. (2019) **Genome-wide Identification and Characterization of a Superfamily of Bacterial Extracellular Contractile Injection Systems** *Cell Rep* **29**:511–521
9. Geller AM, Pollin I, Zlotkin D, Danov A, Nachmias N, Andreopoulos WB, et al. (2021) **The extracellular contractile injection system is enriched in environmental microbes and associates with numerous toxins** *Nat Commun* **12**
10. Basler M, Pilhofer M, Henderson GP, Jensen GJ, Mekalanos JJ (2012) **Type VI secretion requires a dynamic contractile phage tail-like structure** *Nature* **483**:182–6
11. Durand E, Nguyen VS, Zoued A, Logger L, Péhau-Arnaudet G, Aschtgen MS, et al. (2015) **Biogenesis and structure of a type VI secretion membrane core complex** *Nature* **523**:555–60
12. Zachs T, Malit J, Xu J, Schürch A, Sivabalasarma S, Nußbaum P, et al. (2024) **Archaeal type six secretion system mediates contact-dependent antagonism** *bioRxiv*
13. Xu J, Ericson CF, Lien YW, Rutaganira FUN, Eisenstein F, Feldmüller M, et al. (2022) **Identification and structure of an extracellular contractile injection system from the marine bacterium *Algoriphagus machipongonensis*** *Nat Microbiol* **7**:397–410
14. Shikuma NJ, Pilhofer M, Weiss GL, Hadfield MG, Jensen GJ, Newman DK (2014) **Marine tubeworm metamorphosis induced by arrays of bacterial phage tail-like structures** *Science* **343**:529–33

15. Hurst MRH, Beard SS, Jackson TA, Jones SM (2007) **Isolation and characterization of the *Serratia entomophila* antifeeding prophage** *FEMS Microbiol Lett* **270**:42–8
16. Jiang F, Li N, Wang X, Cheng J, Huang Y, Yang Y, et al. (2019) **Cryo-EM Structure and Assembly of an Extracellular Contractile Injection System** *Cell* **177**:370–383
17. Weiss GL, Eisenstein F, Kieninger AK, Xu J, Minas HA, Gerber M, et al. (2022) **Structure of a thylakoid-anchored contractile injection system in multicellular cyanobacteria** *Nat Microbiol* **7**:386–96
18. Casu B, Sallmen JW, Schlimpert S, Pilhofer M (2023) **Cytoplasmic contractile injection systems mediate cell death in *Streptomyces*** *Nat Microbiol* **8**:711–26
19. Vladimirov M, Zhang RX, Mak S, Nodwell JR, Davidson AR (2023) **A contractile injection system is required for developmentally regulated cell death in *Streptomyces coelicolor*** *Nat Commun* **14**
20. Nagakubo T, Yamamoto T, Asamizu S, Toyofuku M, Nomura N, Onaka H (2021) **Phage tail-like nanostructures affect microbial interactions between *Streptomyces* and fungi** *Sci Rep* **11**
21. Nagakubo T, Asamizu S, Yamamoto T, Kato M, Nishiyama T, Toyofuku M, et al. (2023) **Intracellular Phage Tail-Like Nanostructures Affect Susceptibility of *Streptomyces lividans* to Osmotic Stress** *mSphere* **8**:e00114–23
22. Nagakubo T, Nishiyama T, Yamamoto T, Nomura N, Toyofuku M (2024) **Contractile injection systems facilitate sporogenic differentiation of *Streptomyces davawensis* through the action of a phage tapemeasure protein-related effector** *Nat Commun* **15**
23. Schlimpert S, Elliot MA (2023) **The Best of Both Worlds—*Streptomyces coelicolor* and *Streptomyces venezuelae* as Model Species for Studying Antibiotic Production and Bacterial Multicellular Development** *J Bacteriol* **205**:e00153–23
24. Flärdh K, Buttner MJ (2009) ***Streptomyces* morphogenetics: dissecting differentiation in a filamentous bacterium** *Nat Rev Microbiol* **7**:36–49
25. Desfosses A, Venugopal H, Joshi T, Felix J, Jessop M, Jeong H, et al. (2019) **Atomic structures of an entire contractile injection system in both the extended and contracted states** *Nat Microbiol* **4**:1885–94
26. Rybakova D, Schramm P, Mitra AK, Hurst MRH (2015) **Afp14 is involved in regulating the length of Anti-feeding prophage (Afp)** *Mol Microbiol* **96**:815–26
27. Ge P, Scholl D, Prokhorov NS, Avaylon J, Shneider MM, Browning C, et al. (2020) **Action of a minimal contractile bactericidal nanomachine** *Nature* **580**:658–62
28. Jumper J, Evans R, Pritzel A, Green T, Figurnov M, Ronneberger O, et al. (2021) **Highly accurate protein structure prediction with AlphaFold** *Nature* **596**:583–9
29. Alexeyev MF, Winkler HH (1999) **Membrane topology of the *Rickettsia prowazekii* ATP/ADP translocase revealed by novel dual pho-lac reporters 1** Edited by G. von Heijne *J Mol Biol* **285**:1503–13

30. Ramos-León F, Bush MJ, Sallmen JW, Chandra G, Richardson J, Findlay KC, et al., Kana BD, Garner EC (2021) **A conserved cell division protein directly regulates FtsZ dynamics in filamentous and unicellular actinobacteria** *eLife* **10**
31. Bibb MJ, Domonkos A, Chandra G, Buttner MJ (2012) **Expression of the chaplin and rodlin hydrophobic sheath proteins in *Streptomyces venezuelae* is controlled by σ (BldN) and a cognate anti-sigma factor, RsbN** *Mol Microbiol* **84**:1033–49
32. Malpartida F, Hopwood DA (1984) **Molecular cloning of the whole biosynthetic pathway of a *Streptomyces* antibiotic and its expression in a heterologous host** *Nature* **309**:462–4
33. Tsao SW, Rudd BA, He XG, Chang CJ, Floss HG (1985) **Identification of a red pigment from *Streptomyces coelicolor* A3(2) as a mixture of prodigiosin derivatives** *J Antibiot (Tokyo)* **38**:128–31
34. Rapisarda C, Cherrak Y, Kooger R, Schmidt V, Pellarin R, Logger L, et al. (2019) **In situ and high-resolution cryo-EM structure of a bacterial type VI secretion system membrane complex** *EMBO J* **38**
35. Lien YW, Amendola D, Lee KS, Bartlau N, Xu J, Furusawa G, et al. (2024) **Mechanism of bacterial predation via ixotrophy** *bioRxiv*
36. Bongiovanni TR, Latario CJ, Le Cras Y, Trus E, Robitaille S, Swartz K, et al. (2024) **Assembly of a unique membrane complex in type VI secretion systems of Bacteroidota** *Nat Commun* **15**
37. Ouyang R, Ongena V, Muok A, Claessen D, Briegel A (2024) **Phage fibers and spikes: a nanoscale Swiss army knife for host infection** *Curr Opin Microbiol* **77**
38. Weiss GL, Eisenstein F, Kieninger AK, Xu J, Minas HA, Gerber M, et al. (2022) **Structure of a thylakoid-anchored contractile injection system in multicellular cyanobacteria** *Nat Microbiol* **7**:386–96
39. McLean TC (2024) **LazyAF, a pipeline for accessible medium-scale in silico prediction of protein-protein interactions**
40. Kieser T., Bibb M. J., Buttner M. J., Chater K. F., Hopwood D. A. (2000) **Practical *Streptomyces* Genetics** Norwich: John Innes Foundation
41. Gust B, Challis GL, Fowler K, Kieser T, Chater KF (2003) **PCR-targeted *Streptomyces* gene replacement identifies a protein domain needed for biosynthesis of the sesquiterpene soil odor geosmin** *Proc Natl Acad Sci U S A* **100**:1541–6
42. Gust B, Chandra G, Jakimowicz D, Yuqing T, Bruton CJ, Chater KF (2004) **Lambda red-mediated genetic manipulation of antibiotic-producing *Streptomyces*** *Adv Appl Microbiol* **54**:107–28
43. Ohi M, Li Y, Cheng Y, Walz T (2004) **Negative Staining and Image Classification - Powerful Tools in Modern Electron Microscopy** *Biol Proced Online* **6**:23–34
44. Bush MJ, Bibb MJ, Chandra G, Findlay KC, Buttner MJ (2013) **Genes Required for Aerial Growth, Cell Division, and Chromosome Segregation Are Targets of WhiA before Sporulation in *Streptomyces venezuelae*** *mBio* **4**:e00684–13
45. Gallego JJ, Severi E, Chandra G, Palmer T. (2024) **Identification of novel tail--anchored membrane proteins integrated by the bacterial twin--arginine translocase** *Microbiology*

46. Zheng SQ, Palovcak E, Armache JP, Verba KA, Cheng Y, Agard DA (2017) **MotionCor2: anisotropic correction of beam-induced motion for improved cryo-electron microscopy** *Nat Methods* **14**:331–2
47. Afanasyev P, Ravelli RBG, Matadeen R, De Carlo S, van Duinen G, Alewijnse B, et al. (2015) **A posteriori correction of camera characteristics from large image data sets** *Sci Rep* **5**
48. Afanasyev P. (2023) **CryoEM tools**
49. Punjani A, Rubinstein JL, Fleet DJ, Brubaker MA (2017) **cryoSPARC: algorithms for rapid unsupervised cryo-EM structure determination** *Nat Methods* **14**:290–6
50. Wagner T, Merino F, Stabrin M, Moriya T, Antoni C, Apelbaum A, et al. (2019) **SPHIRE-crYOLO is a fast and accurate fully automated particle picker for cryo-EM** *Commun Biol* **2**:1–13
51. Scheres SHW (2012) **RELION: implementation of a Bayesian approach to cryo-EM structure determination** *J Struct Biol* **180**:519–30
52. Weiss GL, Medeiros JM, Pilhofer M (2017) **In Situ Imaging of Bacterial Secretion Systems by Electron Cryotomography** *Methods Mol Biol Clifton NJ* **1615**:353–75
53. Mastronarde DN (2005) **Automated electron microscope tomography using robust prediction of specimen movements** *J Struct Biol* **152**:36–51
54. Kremer JR, Mastronarde DN, McIntosh JR (1996) **Computer visualization of three-dimensional image data using IMOD** *J Struct Biol* **116**:71–6
55. Tegunov D, Cramer P (2019) **Real-time cryo-electron microscopy data preprocessing with Warp** *Nat Methods* **16**:1146–52
56. Emsley P, Lohkamp B, Scott WG, Cowtan K (2010) **Features and development of Coot** *Acta Crystallogr D Biol Crystallogr* **66**:486–501
57. Song Y, DiMaio F, Wang RYR, Kim D, Miles C, Brunette T, et al. (2013) **High-resolution comparative modeling with RosettaCM** *Struct Lond Engl* **21**:1735–42
58. Adams PD, Afonine PV, Bunkóczi G, Chen VB, Davis IW, Echols N, et al. (2010) **PHENIX: a comprehensive Python-based system for macromolecular structure solution** *Acta Crystallogr D Biol Crystallogr* **66**:213–21
59. Schindelin J, Arganda-Carreras I, Frise E, Kaynig V, Longair M, Pietzsch T, et al. (2012) **Fiji - an Open Source platform for biological image analysis** *Nat Methods* **9** <https://doi.org/10.1038/nmeth.2019>
60. Ef P, Td G, Cc H, Gs C, Dm G, Ec M, et al. (2004) **UCSF Chimera--a visualization system for exploratory research and analysis** *J Comput Chem* **25**
61. Goddard TD, Huang CC, Meng EC, Pettersen EF, Couch GS, Morris JH, et al. (2018) **UCSF ChimeraX: Meeting modern challenges in visualization and analysis** *Protein Sci Publ Protein Soc* **27**:14–25
62. Mirdita M, Schütze K, Moriwaki Y, Heo L, Ovchinnikov S, Steinegger M (2022) **ColabFold: making protein folding accessible to all** *Nat Methods* **19**:679–82

63. O'Reilly FJ, Graziadei A, Forbrig C, Bremenkamp R, Charles K, Lenz S, et al. (2023) **Protein complexes in cells by AI -assisted structural proteomics** *Mol Syst Biol* **19**
64. Madeira F, Madhusoodanan N, Lee J, Eusebi A, Niewielska A, Tivey ARN, et al. (2024) **The EMBL-EBI Job Dispatcher sequence analysis tools framework in 2024** *Nucleic Acids Res* **52**:W521–5
65. Zhang Y, Wang L, Zhang S, Yang H, Tan H (2008) **hmgA, transcriptionally activated by HpdA, influences the biosynthesis of actinorhodin in Streptomyces coelicolor** *FEMS Microbiol Lett* **280**:219–25

Author information

Bastien Casu

Department of Biology, Institute of Molecular Biology & Biophysics, Eidgenössische Technische Hochschule Zürich, Zürich, Switzerland
ORCID iD: [0000-0003-3508-6804](https://orcid.org/0000-0003-3508-6804)

Joseph W Sallmen

John Innes Center, Department of Molecular Microbiology, Norwich Research Park, Norwich, United Kingdom
ORCID iD: [0000-0002-5041-299X](https://orcid.org/0000-0002-5041-299X)

Peter E Haas

Department of Biology, Institute of Molecular Biology & Biophysics, Eidgenössische Technische Hochschule Zürich, Zürich, Switzerland
ORCID iD: [0009-0009-9685-0846](https://orcid.org/0009-0009-9685-0846)

Govind Chandra

Department of Biology, Institute of Molecular Biology & Biophysics, Eidgenössische Technische Hochschule Zürich, Zürich, Switzerland
ORCID iD: [0000-0002-7882-6676](https://orcid.org/0000-0002-7882-6676)

Pavel Afanasyev

Department of Biology, Institute of Molecular Biology & Biophysics, Eidgenössische Technische Hochschule Zürich, Zürich, Switzerland
ORCID iD: [0000-0002-6353-6895](https://orcid.org/0000-0002-6353-6895)

Jingwei Xu

Department of Biology, Institute of Molecular Biology & Biophysics, Eidgenössische Technische Hochschule Zürich, Zürich, Switzerland
ORCID iD: [0000-0003-1833-1513](https://orcid.org/0000-0003-1833-1513)

Susan Schlimpert

John Innes Center, Department of Molecular Microbiology, Norwich Research Park, Norwich, United Kingdom
ORCID iD: [0000-0001-6364-8056](https://orcid.org/0000-0001-6364-8056)

For correspondence: Susan.Schlimpert@jic.ac.uk

Martin Pilhofer

Department of Biology, Institute of Molecular Biology & Biophysics, Eidgenössische Technische Hochschule Zürich, Zürich, Switzerland
ORCID iD: [0000-0002-3649-3340](https://orcid.org/0000-0002-3649-3340)

For correspondence: pilhofer@biol.ethz.ch

Editors

Reviewing Editor

Bavesh Kana

University of the Witwatersrand, Johannesburg, South Africa

Senior Editor

Bavesh Kana

University of the Witwatersrand, Johannesburg, South Africa

Reviewer #1 (Public review):

Contractile Injection Systems (CIS) are versatile machines that can form pores in membranes or deliver effectors. They can act extra or intracellularly. When intracellular they are positioned to face the exterior of the cell and hence should be anchored to the cell envelope. The authors previously reported the characterization of a CIS in *Streptomyces coelicolor*, including significant information on the architecture of the apparatus. However, how the tubular structure is attached to the envelope was not investigated. Here they provide a wealth of evidence to demonstrate that a specific gene within the CIS gene cluster, *cisA*, encodes a membrane protein that anchors the CIS to the envelope. More specifically, they show that:

- *CisA* is not required for assembly of the structure but is important for proper contraction and CIS-mediated cell death
- *CisA* is associated to the membrane (fluorescence microscopy, cell fractionation) through a transmembrane segment (*lacZ-phoA* topology fusions in *E. coli*)
- Structural prediction of interaction between *CisA* and a CIS baseplate component
- In addition they provide a high-resolution model structure of the >750-polypeptide *Streptomyces* CIS in its extended conformation, revealing new details of this fascinating machine, notably in the baseplate and cap complexes.

All the experiments are well controlled including trans-complemented of all tested phenotypes.

One important information we miss is the oligomeric state of *CisA*.

While it would have been great to test the interaction between *CisA* and *Cis11*, to perform cryo-electron microscopy assays of detergent-extracted CIS structures to maintain the interaction with *CisA*, I believe that the toxicity of *CisA* upon overexpression or upon expression in *E. coli* render these studies difficult and will require a significant amount of time and optimization to be performed. It is worth mentioning that this study is of significant novelty in the CIS field because, except for Type VI secretion systems, very few membrane proteins or complexes responsible for CIS attachment have been identified and studied.

<https://doi.org/10.7554/eLife.104064.1.sa3>

Reviewer #2 (Public review):

Summary:

The overall question that is addressed in this study is how the *S. coelicolor* contractile injection system (CISSc) works and affects both cell viability and differentiation, which it has been implicated to do in previous work from this group and others. The CISSc system has been enigmatic in the sense that it is free-floating in the cytoplasm in an extended form and is seen in contracted conformation (i.e. after having been triggered) mainly in dead and partially lysed cells, suggesting involvement in some kind of regulated cell death. So, how do the structure and function of the CISSc system compare to those of related CIS from other bacteria, does it interact with the cytoplasmic membrane, how does it do that, and is the membrane interaction involved in the suggested role in stress-induced, regulated cell death? The authors address these questions by investigating the role of a membrane protein, CisA, that is encoded by a gene in the CIS gene cluster in *S. coelicolor*. Further, they analyse the structure of the assembled CISSc, purified from the cytoplasm of *S. coelicolor*, using single-particle cryo-electron microscopy.

Strengths:

The beautiful visualisation of the CIS system both by cryo-electron tomography of intact bacterial cells and by single-particle electron microscopy of purified CIS assemblies are clearly the strengths of the paper, both in terms of methods and results. Further, the paper provides genetic evidence that the membrane protein CisA is required for the contraction of the CISSc assemblies that are seen in partially lysed or ghost cells of the wild type. The conclusion that CisA is a transmembrane protein and the inferred membrane topology are well supported by experimental data. The cryo-EM data suggest that CisA is not a stable part of the extended form of the CISSc assemblies. These findings raise the question of what CisA does.

Weaknesses:

The investigations of the role of CisA in function, membrane interaction, and triggering of contraction of CIS assemblies, are important parts of the paper and are highlighted in the title. However, the experimental data provided to answer these questions appear partially incomplete and not as conclusive as one would expect.

The stress-induced loss of viability is only monitored with one method: an *in vivo* assay where cytoplasmic sfGFP signal is compared to FM5-95 membrane stain. Addition of a sublethal level of nisin lead to loss of sfGFP signal in individual hyphae in the WT, but not in the *cisA* mutant (similarly to what was previously reported for a CIS-negative mutant). Technically, this experiment and the example images that are shown give rise to some concern. Only individual hyphal fragments are shown that do not look like healthy and growing *S. coelicolor* hyphae. Under the stated growth conditions, *S. coelicolor* strains would normally have grown as dense hyphal pellets. It is therefore surprising that only these unbranched hyphal fragments are shown in Fig. 4ab. Further, *S. coelicolor* would likely be in a stationary phase when grown 48 h in the rich medium that is stated, giving rise to concern about the physiological state of the hyphae that were used for the viability assay. It would be valuable to know whether actively growing mycelium is affected in the same way by the nisin treatment, and also whether the cell death effect could be detected by other methods.

The model presented in Fig. 5 suggests that stress leads to a CisA-dependent attachment of CIS assemblies to the cytoplasmic membrane, and then triggering of contraction, leading to cell death. This model makes testable predictions that have not been challenged experimentally. Given that sublethal doses of nisin seem to trigger cell death, there appear to be possibilities to monitor whether activation of the system (via CisA?) indeed leads to at least temporally

increased interaction of CIS with the membrane. Further, would not the model predict that stress leads to an increased number of contracted CIS assemblies in the cytoplasm? No clear difference in length of the isolated assemblies if Fig. S7 is seen between untreated and nisin-exposed cells, and also no difference between assemblies from WT and *cisA* mutant hyphae.

The interaction of CisA with the CIS assembly is critical for the model but is only supported by AlphaFold modelling, predicting interaction between cytoplasmic parts of CisA and Cis11 protein in the baseplate wedge. An experimental demonstration of this interaction would have strengthened the conclusions.

The *cisA* mutant showed a similarly accelerated sporulation as was previously reported for CIS-negative strains, which supports the conclusion that CisA is required for function of CISSc. But the results do not add any new insights into how CIS/CisA affects the progression of the developmental life cycle and whether this effect has anything to do with the regulated cell death that is caused by CIS. The same applies to the effect on secondary metabolite production, with no further mechanistic insights added, except reporting similar effects of CIS and CisA inactivations.

Concluding remarks:

The work will be of interest to anyone interested in contractile injection systems, T6SS, or similar machineries, as well for people working on the biology of streptomyces. There is also a potential impact of the work in the understanding of how such molecular machineries could have been co-opted during evolution to become a mechanism for regulated cell death. However, this latter aspect remains still poorly understood. Even though this paper adds excellent new structural insights and identifies a putative membrane anchor, it remains elusive how the *Streptomyces* CIS may lead to cell death. It is also unclear what the advantage would be to trigger death of hyphal compartments in response to stress, as well as how such cell death may impact (or accelerate) the developmental progression. Finally, it is inescapable to wonder whether the *Streptomyces* CIS could have any role in protection against phage infection.

<https://doi.org/10.7554/eLife.104064.1.sa2>

Reviewer #3 (Public review):

Summary:

In this work, Casu et al. have reported the characterization of a previously uncharacterized membrane protein CisA encoded in a non-canonical contractile injection system of *Streptomyces coelicolor*, CISSc, which is a cytosolic CISs significantly distinct from both intracellular membrane-anchored T6SSs and extracellular CISs. The authors have presented the first high-resolution structure of extended CISSc structure. It revealed important structural insights in this conformational state. To further explore how CISSc interacted with cytoplasmic membrane, they further set out to investigate CisA that was previously hypothesized to be the membrane adaptor. However, the structure revealed that it was not associated with CISSc. Using fluorescence microscope and cell fractionation assay, the authors verified that CisA is indeed a membrane-associated protein. They further determined experimentally that CisA had a cytosolic N-terminal domain and a periplasmic C-terminus. The functional analysis of *cisA* mutant revealed that it is not required for CISSc assembly but is essential for the contraction, as a result, the deletion significantly affects CISSc-mediated cell death upon stress, timely differentiation, as well as secondary metabolite production. Although the work did not resolve the mechanistic detail how CisA interacts with CISSc structure, it provides solid data and a strong foundation for future investigation toward understanding the mechanism of CISSc contraction, and potentially, the relation between the membrane association of CISSc, the sheath contraction and the cell death.

Strengths:

The paper is well-structured, and the conclusion of the study is supported by solid data and careful data interpretation was presented. The authors provided strong evidence on (1) the high-resolution structure of extended CISSc determined by cryo-EM, and the subsequent comparison with known eCIS structures, which sheds light on both its similarity and different features from other subtypes of eCISs in detail; (2) the topological features of CisA using fluorescence microscopic analysis, cell fractionation and PhoA-LacZ α reporter assays, (3) functions of CisA in CISSc-mediated cell death and secondary metabolite production, likely via the regulation of sheath contraction.

Weaknesses:

The data presented are not sufficient to provide mechanistic details of CisA-mediated CISSc contraction, as authors are not able to experimentally demonstrate the direct interaction between CisA with baseplate complex of CISSc (hypothesized to be via Cis11 by structural modeling), since they could not express cisA in *E. coli* due to its potential toxicity. Therefore, there is a lack of biochemical analysis of direct interaction between CisA and baseplate wedge. In addition, there is no direct evidence showing that CisA is responsible for tethering CISSc to the membrane upon stress, and the spatial and temporal relation between membrane association and contraction remains unclear. Further investigation will be needed to address these questions in future.

Discussion:

Overall, the work provides a valuable contribution to our understanding on the structure of a much less understood subtype of CISs, which is unique compared to both membrane-anchored T6SSs and host-membrane targeting eCISs. Importantly, the work serves as a good foundation to further investigate how the sheath contraction works here. The work contributes to expanding our understanding of the diverse CIS superfamilies.

<https://doi.org/10.7554/eLife.104064.1.sa1>

Author response:

We thank the editor and the three reviewers for the positive assessment and constructive feedback on how to improve our manuscript. We greatly appreciate that our work is considered valuable to the field, the recognition of the high-resolution model we presented, and the comments on our investigation of CisA's role in the attachment and firing mechanism of the extended assembly. It is truly gratifying to know that our study contributes to expanding the current understanding of the biology of *Streptomyces* and the role of these functionally diverse and fascinating bacterial nanomachines.

We have provided specific responses to each reviewer's comments below. In summary, we intend to address the following requested revisions:

We will expand our bioinformatic analysis of CisA and provide additional information on the oligomeric state of CisA. We will also modify the text, figures, and figure legends to improve the clarity of our work and experimental procedures.

Some reviewer comments would require additional experimental work, some of which would involve extensive optimization of experimental conditions. Because both lead postdoctoral researchers involved in this work have now left the lab, we currently do not have the capability to perform additional experimental work.

Reviewer #1 (Public review):

*Contractile Injection Systems (CIS) are versatile machines that can form pores in membranes or deliver effectors. They can act extra or intracellularly. When intracellular they are positioned to face the exterior of the cell and hence should be anchored to the cell envelope. The authors previously reported the characterization of a CIS in *Streptomyces coelicolor*, including significant information on the architecture of the apparatus. However, how the tubular structure is attached to the envelope was not investigated. Here they provide a wealth of evidence to demonstrate that a specific gene within the CIS gene cluster, *cisA*, encodes a membrane protein that anchors the CIS to the envelope. More specifically, they show that:*

*- *CisA* is not required for assembly of the structure but is important for proper contraction and CIS-mediated cell death*

*- *CisA* is associated to the membrane (fluorescence microscopy, cell fractionation) through a transmembrane segment (*lacZ-phoA* topology fusions in *E. coli*)*

*- Structural prediction of interaction between *CisA* and a CIS baseplate component*

*- In addition they provide a high-resolution model structure of the >750-polypeptide *Streptomyces* CIS in its extended conformation, revealing new details of this fascinating machine, notably in the baseplate and cap complexes.*

All the experiments are well controlled including trans-complemented of all tested phenotypes.

*One important information we miss is the oligomeric state of *CisA*.*

*While it would have been great to test the interaction between *CisA* and *Cis11*, to perform cryo-electron microscopy assays of detergent-extracted CIS structures to maintain the interaction with *CisA*, I believe that the toxicity of *CisA* upon overexpression or upon expression in *E. coli* render these studies difficult and will require a significant amount of time and optimization to be performed. It is worth mentioning that this study is of significant novelty in the CIS field because, except for Type VI secretion systems, very few membrane proteins or complexes responsible for CIS attachment have been identified and studied.*

We thank this reviewer for their highly supportive and positive comments on our manuscript. We are grateful for this reviewer's recognition of the novelty of our study, particularly in the context of membrane proteins and complexes involved in CIS attachment.

We agree that further experimental evidence on the direct interaction between *CisA* and *Cis11* would have strengthened our model of *CisA* function. However, as noted by this reviewer, this additional work is technically challenging and currently beyond the scope of this study.

We thank Reviewer #1 for suggesting discussing the potential oligomeric state of *CisA*. We will perform additional AlphaFold modelling of *CisA* and discuss the result of this analysis in the revised manuscript.

Reviewer #2 (Public review):

Summary:

*The overall question that is addressed in this study is how the *S. coelicolor* contractile injection system (CISSc) works and affects both cell viability and differentiation, which it*

*has been implicated to do in previous work from this group and others. The CISSc system has been enigmatic in the sense that it is free-floating in the cytoplasm in an extended form and is seen in contracted conformation (i.e. after having been triggered) mainly in dead and partially lysed cells, suggesting involvement in some kind of regulated cell death. So, how do the structure and function of the CISSc system compare to those of related CIS from other bacteria, does it interact with the cytoplasmic membrane, how does it do that, and is the membrane interaction involved in the suggested role in stress-induced, regulated cell death? The authors address these questions by investigating the role of a membrane protein, CisA, that is encoded by a gene in the CIS gene cluster in *S. coelicolor*. Further, they analyse the structure of the assembled CISSc, purified from the cytoplasm of *S. coelicolor*, using single-particle cryo-electron microscopy.*

Strengths:

The beautiful visualisation of the CIS system both by cryo-electron tomography of intact bacterial cells and by single-particle electron microscopy of purified CIS assemblies are clearly the strengths of the paper, both in terms of methods and results. Further, the paper provides genetic evidence that the membrane protein CisA is required for the contraction of the CISSc assemblies that are seen in partially lysed or ghost cells of the wild type. The conclusion that CisA is a transmembrane protein and the inferred membrane topology are well supported by experimental data. The cryo-EM data suggest that CisA is not a stable part of the extended form of the CISSc assemblies. These findings raise the question of what CisA does.

We thank Reviewer #2 for the overall positive evaluation of our manuscript and the constructive criticism.

Weaknesses:

The investigations of the role of CisA in function, membrane interaction, and triggering of contraction of CIS assemblies, are important parts of the paper and are highlighted in the title. However, the experimental data provided to answer these questions appear partially incomplete and not as conclusive as one would expect.

We acknowledge that some aspects of our work have not been fully answered. We believe that providing additional experimental data is currently beyond the scope of this study. To improve this study, we will modify the text and clarify experimental procedures and figures where possible in the revised version of our manuscript.

*The stress-induced loss of viability is only monitored with one method: an in vivo assay where cytoplasmic sfGFP signal is compared to FM5-95 membrane stain. Addition of a sublethal level of nisin lead to loss of sfGFP signal in individual hyphae in the WT, but not in the cisA mutant (similarly to what was previously reported for a CIS-negative mutant). Technically, this experiment and the example images that are shown give rise to some concern. Only individual hyphal fragments are shown that do not look like healthy and growing *S. coelicolor* hyphae. Under the stated growth conditions, *S. coelicolor* strains would normally have grown as dense hyphal pellets. It is therefore surprising that only these unbranched hyphal fragments are shown in Fig. 4ab.*

We thank Reviewer #2 for their thoughtful criticism regarding our stress-induced viability assay and the data presented in Figure 4. We acknowledge the importance of ensuring that the presented images should reflect the physiological state of *S. coelicolor* under the stated growth conditions and recognize that hyphal fragments shown in Figure 4 do not fully capture the typical morphology of *S. coelicolor*. As pointed out by this reviewer, *S. coelicolor* grows in large hyphal clumps when cultured in liquid media, making the quantification of

fluorescence intensities in hyphae expressing cytoplasmic GFP and stained with the membrane dye FM5-95 particularly challenging. To improve the image analysis and quantification of GFP and FM5-95-fluorescent intensities across the three *S. coelicolor* strains (wildtype, *cisA* deletion mutant and the complemented *cisA* mutant), we vortexed the cell samples briefly before imaging to break up hyphal clumps, increasing hyphal fragments. The hyphae shown in our images were selected as representative examples across three biological replicates.

Further, S. coelicolor would likely be in a stationary phase when grown 48 h in the rich medium that is stated, giving rise to concern about the physiological state of the hyphae that were used for the viability assay. It would be valuable to know whether actively growing mycelium is affected in the same way by the nisin treatment, and also whether the cell death effect could be detected by other methods.

The reasoning behind growing *S. coelicolor* for 48 h before performing the fluorescence-based viability assay was that we (DOI: 10.1038/s41564-023-01341-x) and others (e.g.: DOI: 10.1038/s41467-023-37087-7) previously showed that the levels of CIS particles peak at the transition from vegetative to reproductive/stationary growth, thus indicating that CIS activity is highest during this growth stage. The obtained results in this manuscript are in agreement with our previous study, in which we showed a similar effect on the viability of wildtype versus *cis*-deficient *S. coelicolor* strains (DOI: 10.1038/s41564-023-01341-x) using nisin, the protonophore CCCP and UV light, and supported by biological replicate experiments and appropriate controls. Furthermore, our results are in agreement with the findings reported in a complementary study by Vladimirov et al. (DOI: 10.1038/s41467-023-37087-7) that used a different approach (SYTO9/PI staining of hyphal pellets) to demonstrate that CIS-deficient mutants exhibit decreased hyphal death. We agree that it would be interesting to test if actively growing hyphae respond differently to nisin treatment, and such experiments will be considered in future work.

Taken together, we believe that the results obtained from our fluorescence-based viability assay are consistent with data reported by others and provide strong experimental evidence that functional CIS mediate hyphal cell death.

The model presented in Fig. 5 suggests that stress leads to a CisA-dependent attachment of CIS assemblies to the cytoplasmic membrane, and then triggering of contraction, leading to cell death. This model makes testable predictions that have not been challenged experimentally. Given that sublethal doses of nisin seem to trigger cell death, there appear to be possibilities to monitor whether activation of the system (via CisA?) indeed leads to at least temporally increased interaction of CIS with the membrane.

We thank this reviewer for their suggestions on how to test our model further. In the meantime, we have performed co-immunoprecipitation experiments using *S. coelicolor* cells that produced CisA-FLAG as bait and were treated with a sub-lethal nisin concentration for 0/15/45 min. Mass spectrometry analysis of co-eluted peptides did not show the presence of CIS-associated peptides. While we cannot exclude the possibility that our experimental assay requires further optimization to successfully demonstrate a CisA-CIS interaction (e.g. optimization of the use of detergents to improve the solubilization of CisA from *Streptomyces* membrane, which is currently not an established method), an alternative and equally valid hypothesis is that the interaction between CIS particles and CisA is transient and therefore difficult to capture. We would like to mention that we did detect CisA peptides in crude purifications of CIS particles from nisin-stressed cells (Supplementary Table 2, manuscript: line 265/266), supporting our model that CisA associates with CIS particles *in vivo*.

Further, would not the model predict that stress leads to an increased number of contracted CIS assemblies in the cytoplasm? No clear difference in length of the isolated assemblies if Fig. S7 is seen between untreated and nisin-exposed cells, and also no difference between assemblies from WT and cisA mutant hyphae.

The reviewer is correct that there is no clear difference in length in the isolated CIS particles shown in Figure S7. This is in line with our results, which show that CisA is not required for the correct assembly of CIS particles and their ability to contract in the presence and absence of nisin treatment. The purpose of Figure S7 was to support this statement. We would like to note that the particles shown in Figure S7 were purified from cell lysates using a crude sheath preparation protocol, during which CIS particles generally contract irrespective of the presence or absence of CisA. Thus, we cannot comment on whether there is an increased number of contracted CIS assemblies in the cytoplasm of nisin-exposed cells. To answer this point, we would need to acquire additional cryo-electron tomograms (cryoET) of the different strains treated with nisin. We appreciate this reviewer's suggestions. However, cryoET is an extremely time and labour-intensive task, and given that we currently don't know the exact dynamics of the CIS-CisA interaction following exogenous stress, we believe this experiment is beyond the scope of this work.

The interaction of CisA with the CIS assembly is critical for the model but is only supported by Alphafold modelling, predicting interaction between cytoplasmic parts of CisA and Cis11 protein in the baseplate wedge. An experimental demonstration of this interaction would have strengthened the conclusions.

We agree that direct experimental evidence of this interaction would have further strengthened the conclusions of our study, and we have extensively tried to provide additional experimental evidence. Unfortunately, due to the toxicity of CisA expression in *E. coli* and the transient nature of the interaction under our experimental conditions, we were unable to pursue direct biochemical or biophysical validation methods, such as co-purification or bacterial two-hybrid assays. While these challenges limited our ability to experimentally confirm the interaction, the AlphaFold predictions provided a valuable hypothesis and mechanistic insight into the role of CisA.

The cisA mutant showed a similarly accelerated sporulation as was previously reported for CIS-negative strains, which supports the conclusion that CisA is required for function of CISSc. But the results do not add any new insights into how CIS/CisA affects the progression of the developmental life cycle and whether this effect has anything to do with the regulated cell death that is caused by CIS. The same applies to the effect on secondary metabolite production, with no further mechanistic insights added, except reporting similar effects of CIS and CisA inactivations.

We thank this reviewer for their thoughtful feedback and for highlighting the connections between CisA, CIS function, and their effects on the developmental life cycle and secondary metabolite production in *S. coelicolor*. The main focus of this study was to provide further insight into how CIS contraction and firing are mediated in *Streptomyces*, and we used the analysis of accelerated sporulation and secondary metabolite production to assess the functionality of CIS in the presence or absence of CisA.

We agree that we still don't fully understand the nature of the signals that trigger CIS contraction, but we do know that the production of CIS assemblies seems to be an integral part of the *Streptomyces* multicellular life cycle as demonstrated in two independent previous studies (DOI: 10.1038/s41564-023-01341-x and DOI: 10.1038/s41467-023-37087-7). We propose that the assembly and firing of *Streptomyces* CIS particles could present a molecular

mechanism to sacrifice only a part of the mycelium to either prevent the spread of local cellular damage or to provide additional nutrients for the rest of the mycelium and delay the terminal differentiation into spores and affect the production of secondary metabolites.

We recognize the importance of understanding the regulation and mechanistic details underpinning the proposed CIS-mediated regulated cell death model. This will be further explored in future studies.

Concluding remarks:

The work will be of interest to anyone interested in contractile injection systems, T6SS, or similar machineries, as well for people working on the biology of streptomycetes. There is also a potential impact of the work in the understanding of how such molecular machineries could have been co-opted during evolution to become a mechanism for regulated cell death. However, this latter aspect remains still poorly understood. Even though this paper adds excellent new structural insights and identifies a putative membrane anchor, it remains elusive how the Streptomyces CIS may lead to cell death. It is also unclear what the advantage would be to trigger death of hyphal compartments in response to stress, as well as how such cell death may impact (or accelerate) the developmental progression. Finally, it is inescapable to wonder whether the Streptomyces CIS could have any role in protection against phage infection.

We thank Reviewer #2 for their supportive assessment of our work. In the revised manuscript, we will briefly discuss the impact of functional CIS assemblies on Streptomyces development. We previously tested if Streptomyces could defend against phages but have not found any experimental evidence to support this idea. The analysis of phage defense mechanisms is an underdeveloped area in Streptomyces research, partly due to the currently limited availability of a diverse phage panel.

Reviewer #3 (Public review):

Summary:

In this work, Casu et al. have reported the characterization of a previously uncharacterized membrane protein CisA encoded in a non-canonical contractile injection system of Streptomyces coelicolor, CISSc, which is a cytosolic CISs significantly distinct from both intracellular membrane-anchored T6SSs and extracellular CISs. The authors have presented the first high-resolution structure of extended CISSc structure. It revealed important structural insights in this conformational state. To further explore how CISSc interacted with cytoplasmic membrane, they further set out to investigate CisA that was previously hypothesized to be the membrane adaptor. However, the structure revealed that it was not associated with CISSc. Using fluorescence microscope and cell fractionation assay, the authors verified that CisA is indeed a membrane-associated protein. They further determined experimentally that CisA had a cytosolic N-terminal domain and a periplasmic C-terminus. The functional analysis of cisA mutant revealed that it is not required for CISSc assembly but is essential for the contraction, as a result, the deletion significantly affects CISSc-mediated cell death upon stress, timely differentiation, as well as secondary metabolite production. Although the work did not resolve the mechanistic detail how CisA interacts with CISSc structure, it provides solid data and a strong foundation for future investigation toward understanding the mechanism of CISSc contraction, and potentially, the relation between the membrane association of CISSc, the sheath contraction and the cell death.

Strengths:

The paper is well-structured, and the conclusion of the study is supported by solid data and careful data interpretation was presented. The authors provided strong evidence on (1) the high-resolution structure of extended CISSc determined by cryo-EM, and the subsequent comparison with known eCIS structures, which sheds light on both its similarity and different features from other subtypes of eCISs in detail; (2) the topological features of CisA using fluorescence microscopic analysis, cell fractionation and PhoA-LacZa reporter assays, (3) functions of CisA in CISSc-mediated cell death and secondary metabolite production, likely via the regulation of sheath contraction.

Weaknesses:

The data presented are not sufficient to provide mechanistic details of CisA-mediated CISSc contraction, as authors are not able to experimentally demonstrate the direct interaction between CisA with baseplate complex of CISSc (hypothesized to be via Cis11 by structural modeling), since they could not express cisA in E. coli due to its potential toxicity. Therefore, there is a lack of biochemical analysis of direct interaction between CisA and baseplate wedge. In addition, there is no direct evidence showing that CisA is responsible for tethering CISSc to the membrane upon stress, and the spatial and temporal relation between membrane association and contraction remains unclear. Further investigation will be needed to address these questions in future.

We thank Reviewer #3 for the supportive evaluation and constructive criticism of our study in the public and non-public review. We appreciate your recognition of the technical limitations of experimentally demonstrating a direct interaction between CisA and CIS baseplate complex, and we agree that further investigations in the future will hopefully provide a full mechanistic understanding of the spatiotemporal interaction of CisA and CIS particular and the subsequent CIS firing.

To further improve the manuscript, we will revise the text and clarify figures and figure legends as suggested in the non-public review.

Discussion:

Overall, the work provides a valuable contribution to our understanding on the structure of a much less understood subtype of CISs, which is unique compared to both membrane-anchored T6SSs and host-membrane targeting eCISs. Importantly, the work serves as a good foundation to further investigate how the sheath contraction works here. The work contributes to expanding our understanding of the diverse CIS superfamilies.

Thank you.

<https://doi.org/10.7554/eLife.104064.1.sa0>